• NASA CR-159262

NASA Contractor Report 159262

NASA-CR-159262
1981 0011539

A STUDY OF HIGH-ALTITUDE MANNED RESEARCH AIRCRAFT EMPLOYING STRUT-BRACED WINGS OF HIGH-ASPECT-RATIO

Paul M. Smith, John DeYoung, William A. Lovell,
Jack E. Price, and G. Fred Washburn

KENTRON INTERNATIONAL, INC.
an LTV company
Hampton Technical Center
Hampton, Virginia 23666

CONTRACT NAS1-16000

February 1981

National Aeronautics and
Space Administration

Langley Research Center
Hampton, Virginia 23665

LIBRARY COPY

NOV 12 1986

LANGLEY RESEARCH CENTER
LIBRARY, NASA
HAMPTON, VIRGINIA

NF01078

SUMMARY

A study was conducted to determine whether subsonic manned research aircaft utilizing strut-braced wings of high-aspect-ratio had performance improvements when compared to a baseline concept. The effect of increased wing aspect ratio on structural weight, system weight, and maximum range and altitude was determined for configurations with and without strut bracing.

The significant results of the study indicated that an optimum cantilever configuration with a wing aspect ratio of 26 has a 19 percent improvement in cruise range when compared to a baseline concept with a wing aspect ratio of approximately 10. An optimum strut-braced configuration with a wing aspect ratio of 28 has a 31 percent improvement in cruise range when compared to the same baseline concept. The increased improvement in range capability is due to the reduction in wing weight resulting from the use of long, braced struts and the aerodynamic advantages in making these lifting struts. All configurations assume the same mission payload and fuel.

INTRODUCTION

Flight at high altitude and at speeds below the drag divergence Mach number leads to aircraft operation at low dynamic pressure. Although, at the resulting low Reynolds numbers, significant levels of laminar flow can be attained, substantial levels of induced drag can result. Increasing cantilever wing aspect ratio to minimize these induced drag levels results in significant structural weight increases. The use of wing struts can alleviate stress and reduce weight. The use of lifting struts can also offer aerodynamic advantages.

The relative advantages of lifting struts have already been demonstrated for low speed flight. Theoretical studies and wind-tunnel tests by M. Hurel have shown that the induced drag of a monoplane braced with suitably designed lifting struts was less than that of a cantilever monoplane of the same wing span and area. Flight tests were conducted in the early 1950's with the Hurel-Dubois 10, which had an aspect ratio of 32. The results included the achievement of a lift-to-drag ratio of 18 at a lift coefficient of 2.3 and the demonstration of good stability and control characteristics.

N81-20067

This report is concerned with the evaluation of the effect of high-aspect-ratio wings with lifting struts on the performance of jet-powered, high-altitude airplanes. A parametric study is conducted with a common fuselage, engine, fuel load, and wing area. Preliminary structural designs are developed for wings with and without lifting struts at aspect ratios of 20, 25, and 30. One additional configuration with greater wing area is also considered. The drag characteristics of the wings are enhanced with the use of laminar flow (NACA 6-series) airfoils. A method for determining the extent of attainable natural laminar flow is presented in an appendix. Methods for preliminary structural design and for aerodynamic analysis of wings with lifting struts are also given in appendices.

The validity of the analysis and comparison is based in part on the use of a consistent methodology on both the baseline design and the study configurations. The baseline characteristics were compared with available data for the aircraft described in reference 1.

SYMBOLS AND DEFINITIONS

Values are given in both the International System of Units (SI) and U.S. Customary Units. The calculations were made in U.S. Customary Units and then converted to SI units; thus, minor discrepancies in tabulated subtotals and totals of the SI derived units may occur due to rounding off.

A	wing aspect ratio
b	wing span, m (ft)
C_D	drag coefficient
C_{D_c}	compressibility drag coefficient
C_{D_p}	wing profile drag coefficient
$C_{D_{pa}}$	parasite drag coefficient
C_f	flat-plate skin-friction drag coefficient

C_L	lift coefficient
c	airfoil chord length, m (ft)
$\bar{c}$	mean aerodynamic chord, m (ft)
c_d	two-dimensional drag coefficient
c_p	peripheral distance around airfoil chord, m (ft)
D	drag, N (lbf)
e	airplane efficiency factor
e_p	wing potential-flow efficiency factor
L	lift, N (lbf)
ℓ_t	distance from center of gravity to tail $\bar{c}/4$ location, m (ft)
M	Mach number
N_y	root chordwise running load, N/m (lbf/ft)
n_z	normal load factor
P	strut axial load
q	free-stream dynamic pressure, Pa (lbf/ft^2)
R	Reynolds number
S	total wing area, m^2 (ft^2)
S_w	exposed wing wetted area, m^2 (ft^2)
S_v	vertical tail area, m^2 (ft^2)
t/c	airfoil thickness-chord ratio
V_{climb}	climb speed, knots
V_D	dive speed, knots

V_{NE}	never-exceed speed, knots
V_{NO}	normal operating speed, knots
V_g	gust velocity, m/s (ft/s)
Δ	increment
δ	wing-tip deflection, m (in)
δ_f	trailing-edge flap deflection, deg
η	distance along wing as a fraction of semispan, y/(b/2)
λ	wing straight taper ratio

Subscripts:

cs	constant section
lam	laminar
max.	maximum
min.	minimum
s	strut; strut location, y/b/2
t	tip
turb	turbulent
ult	ultimate

AIRCRAFT DEVELOPMENT

Configuration Description

Nine configurations were considered in this study, four with cantilever wings and five with strut-braced wings. The cantilever designs included a baseline configuration and three alternate configurations with progressively higher aspect ratios. The strut-braced designs included four with aspect ratios and areas corresponding to the cantilever wing configurations and one with a larger wing area.

Baseline configuration description. - The baseline configuration, presented in figure 1 and described in reference 1, is a single-place aircraft intended for subsonic high-altitude, long-range operation. It is characterized by a relatively high-aspect-ratio wing (10.32) and tandem landing gear that retracts into the fuselage. Auxiliary gear are located on the underside of each wing and jettisoned on takeoff. It has an all-aluminum airframe and is powered by a single turbojet engine with an uninstalled thrust rating of 75.6 kN (17 000 lbf). Maximum wing fuel represents 92.4 percent of the total fuel. A 2.47 kN (555 lbf) engine feed/collector tank is located in the fuselage. Pertinent dimensional characteristics are presented in table I(a).

Description of alternate configurations. - Assuming a constant wing area of 57.6 m^2 (620 ft^2) , additional configurations with wing aspect ratios of 20, 25, and 30 were developed. Based on DeYoung's work of reference 2, a near optimum planar wing planform was chosen to produce an approximately elliptical spanwise load distribution resulting in wing potential-flow efficiency factors greater than 0.98. The planform had a constant chord to 50 percent of the wing semispan with a 3/11 straight taper outboard to the tip. This planform was used with all configurations except the baseline, cantilever wing configuration. Pertinent dimensional characteristics for the three higher aspect ratio configurations are presented in tables I(b), I(c), and I(d). The horizontal tail characteristics were kept constant while the vertical tail area was increased with increasing wing aspect ratio to maintain a constant relationship between ℓ_t/b times S_v/S.

All alternate configurations had the wing placed on top of the fuselage to facilitate the addition of wing struts attached from the bottom side of the fuselage to the wing. Strut-braced wing configurations were developed for the baseline aspect ratio and for the three higher aspect ratios. In addition, a 92.9 m^2 (1000 ft^2) wing (a 61 percent increase in area) was selected to determine the effect of lowering the operating lift coefficients so that the aircraft could cruise on the front side of the thrust required curve and attain higher operating ceilings. A typical strut-braced configuration, with an aspect ratio of 20, is presented in figure 2.

Aerodynamics Characteristics

In order to make a meaningful assessment of the effect of strut-braced high-aspect-ratio wings on the mission capability of subsonic high-altitude aircraft, it was first necessary to predict the capabilities of the baseline configuration described in reference 1. Capabilities of the alternate configurations were then predicted using a consistent methodology.

Aircraft lift was assumed to be equal to the instantaneous aircraft weight for all flight conditions except climb, where it was assumed to be equal to weight times the cosine of the climb angle.

The drag of the various configurations was estimated by summing the aircraft minimum parasite drag, the increment in parasite drag due to lift, and the induced drag. Friction drag, for 0.70 Mach number and altitude of 12.2 km (40 000 ft), was computed by representing the various components by their appropriate wetted areas and reference lengths. Natural laminar flow was assumed to be present on the forward 30 percent of the fuselage. The percentage for the wing was estimated using appendix A. The resulting wing percentage was reduced by ten percent due to assumed inboard wing flow separation resulting from turbulent flow from the fuselage. The assumed conditions for calculation of turbulent skin friction were smooth flat plate with transition fixed at the leading edge of each component. Form-drag corrections, which include supervelocity and pressure effects, were applied to each of the components as a function of thickness-chord ratio for lifting surfaces and fineness ratio for bodies. Wing-body and tail-body interference drags were estimated using the data from chapter 8 of reference 3.

Additional drag increments were calculated to account for compressibility, speed brakes, and landing gear. The estimated drag increment due to compressibility is presented in figure 3 as a function of Mach number and lift coefficient.

For the strut-braced configurations, the struts are positioned in the flow field of the wing so as to provide a uniform spanload distribution and to be lifting at the same lift coefficient as the wing, based on their respective lifting areas for the 1g design cruise case. The strut contribution to the combined wing-strut induced drag level was determined by the method developed in appendix B, using the actual wing potential-flow efficiency factor as presented

in figure A-4 of appendix A. Analysis of the subsonic wind-tunnel test data of reference 4 indicated that the strut interference drag was 20 percent of the isolated strut drag. Based on this result, the estimated isolated strut drag was increased 20 percent, although in the study of reference 5 only a ten percent increase was used. For the strut contribution to compressibility drag, the data of figure 3 was used and the resulting drag increment factored by the ratio of strut-to-wing wetted areas.

Figures 4 and 5 present estimated values of aerodynamic parameters for the study configurations. Lift-drag polars are given in figure 4 for the cantilever-wing configurations, including the baseline aircraft. Figure 5 presents the estimated lift-drag polars for five strut-braced configurations, four with wing areas of 57.6 m^2 (620 ft^2) and one with a wing area of 92.9 m^2 (1000 ft^2).

Propulsion Characteristics

To conduct the required studies on the subsonic high-altitude research aircraft, compatible engine performance, weight, and size were required. The NASA Langley Research Center provided such data for a typical subsonic turbojet engine capable of operation at high altitude.

Engine performance. - The uninstalled engine performance was corrected for the installation effects for a standard day atmosphere at all operating power conditions. These included an inlet pressure recovery of 0.97, which is typical for the engine installation used in this study, a service airbleed of 0.5 percent of the compressor discharge airflow, and a shaft power extraction of 7.46 kW (10 horsepower) to power aircraft equipment. The resulting installed performance is provided in graphical form for maximum climb power, maximum cruise power, and part-power cruise conditions in figures 6 through 8. Maximum climb thrust and associated fuel flow rate, as a function of pressure altitude and Mach number, are presented in figures 6 and 7, respectively. Maximum and part-power cruise fuel flow rates are presented as a function of thrust and Mach number for cruise pressure altitudes of 19.8 km (65 000 ft) through 24.4 km (80 000 ft) in 1.5 km (5000 ft) increments in figure 8.

Engine weight and dimensions. - The estimated bare engine weight is 22.0 kN (4950 lbf) and does not include the inlet, nozzle, thrust reverser, or mounting brackets for the attachment of aircraft equipment. A sketch of the estimated engine envelope dimensions, center of gravity position, and mounting locations is presented in figure 9.

Structural Characteristics

Since existing weight equations are based on aircraft with relatively low-aspect-ratio wings and there is little weights data available on high-aspect-ratio wings, it was necessary to perform preliminary structural analyses to determine wing weights. Wings with aspect ratios of 10, 20, 25, and 30 were strength sized,and the weights data were used to modify the wing weight prediction equation used in a mass properties computer program. In addition to the strength sizing data, the structural analysis provided maneuver and gust loads as well as flutter and deflection data for use in the structural design. The modified weight prediction method presented herein is adequate for system and configuration studies, but requires further validation for production design.

The design procedure developed for this study consisted of determination of maneuver and ground handling loads; calculation of the strut external loads and wing box internal loads; sizing the struts and wing box for strength to carry maneuver and taxi loads; determination of the weights of the cantilever and strut-braced wings; and estimation of the gust and flutter capability along with wing tip deflection characteristics. The detailed wing and strut weight prediction methods and results as well as the procedures utilized are presented in appendix C.

Simulation and analysis. - A combination of finite element and traditional structural analysis techniques was used in strength sizing the wing and struts. The SPAR Structural Analysis system (ref. 6) was utilized to determine strut external loads and wing internal loads and deflections. The wing skins were sized based on the internal loads. An ultimate load factor of 3.0 and 28.0 kN (6290 lbf) of fuel in the wing were used throughout the study.

The wing is constructed of conventional 7075-T6 aluminum alloy. The wing box consists of wing cover skins stabilized by stringers, full-depth ribs, and two spars located along the 10 percent and 70 percent chord lines. The .15 cm (.06 in.) thick leading- and trailing-edge skins carry only pressure loads and were modeled to carry no wing bending or shear loads. To facilitate the analysis, the spars and ribs were held at a constant gauge, .25 cm (.10 in.). The strut bracing redistributes the loads in the spars and ribs, but this redistribution does not greatly affect the overall wing weight.

A study was conducted to optimize long, braced, lifting struts for minimum configuration weight by structurally sizing the primary bending components using beam-column theory. The details of the methods used are given in appendix C. The struts are attached to the bottom-side of the fuselage and to the lower wing-skin at a wing rib. The struts are stabilized by lateral braces attached to the wing as shown in figure 2.

Aerodynamic and inertial loads. - Airloads were calculated for cruise and at the +2g and -1g maneuver conditions. For both the cantilever and strut-braced wing configurations, airload distributions were constructed midway between the elliptical and actual planform geometry distributions. In each case, the ordinate of the loading was scaled so that each distribution gave the same total load. Betz, in figure J-63 of reference 7, demonstrated that the spanwise loading varied from elliptical to approximately the chord distribution as the aspect ratio was varied from 0 to 10, respectively. Glauert, on page 154 of reference 8, noted, for a wing with an aspect ratio of approximately 6, that the "load grading curve (had a form) intermediate between that of the airfoil and that of the ellipse." Figure 10 presents the assumed wing load distributions. The strut was designed to carry a uniform airload distribution computed at the same lift coefficient as for the wing for the 1g design cruise case.

In general, the wing box is critical for the +2g maneuver condition while the strut is critical for the -1g condition. For this condition the strut must carry combined bending and axial compression loads. The airloads cause the wing to bend which produces the strut axial compression. Strut compression loads were also calculated for the 2g taxi condition. Both rigid body and dynamic components were included. Utilizing a typical landing gear time-history input,

the wing dynamic response loads and deflections were not significant in comparison to the rigid body components.

Structural loads and response. - The effect of variations in strut-attachment location on wing structural loads is shown in figures 11, 12, and 13. These figures indicate that the attachment location has a strong effect on both the distribution and magnitude of both bending moment and shear (figs. 11 and 12, respectively). Since the weight is essentially proportional to the area under the bending moment curves, the strut-braced configurations are lighter than the cantilever configurations, even with the additional strut weight. The maximum bending moments are compared in figure 13 for both the cantilever and strut-braced configurations. For the strut-braced configurations, the wing bending moment (and thus the wing weight) grows less rapidly with aspect ratio than for the cantilever configurations. From a strength standpoint, this means that the higher the aspect ratio,the more beneficial is strut bracing.

The effect of aspect ratio on strut structural design is shown in figures 14 and 15. The strut axial loads are given in figure 14 for three load conditions. The -1g maneuver load condition is the most critical because the strut must carry both axial compression imposed by the wing and the strut airload in bending. For this condition the strut is analyzed as a beam column based on reference 9. The major structural parameters which affect strut location selection are shown in figure 15. The strut located at .4 of the wing semispan was selected for this study as it results in a minimum weight wing box, as signified by the minimum in the N_y curve shown in figure 15. The beneficial effect of utilizing a strut to keep deflections within reasonable limits is illustrated in figure 16.

A preliminary study of gust and wing flutter sensitivity to increasing aspect ratio was conducted. A 3g ultimate load factor was utilized for this study. Figure 17 shows that the configuration has the capability to withstand a gust of slightly less than 7.6 m/sec (25 ft/sec) as calculated by the method given in reference 10, paragraph 25.341. Increasing the vehicle design ultimate load factor, n_z, to 5.0 increases the gust capability to 15. m/sec (50 ft/sec). These data are for a cantilever wing.

A simplified flutter analysis was conducted utilizing the methods given in reference 11. The results, which are shown in figure 18, indicate that the flutter speed decreases with increasing wing aspect ratio for the cantilever wing. For the aspect ratio 20 case shown, the cantilever and strut-braced curves tend to coincide. Based on the methodology used herein for ascertaining airplane flutter, all configurations were assessed to be flutter-free.

Weights Summary

The vehicle group weights, estimated using an unpublished mass properties computer program, and the wing weights, including struts, determined by the methods described in appendix C, are presented in table II and figure 19. These weights data show that strut-braced configurations are lighter than conventional cantilever winged concepts. The strut-braced vehicle with an aspect ratio of 30 is only 4 percent heavier than the baseline cantilever winged vehicle with an aspect ratio of 10.32.

Although all calculations were based on the use of the same value of initial fuel weight, available fuel volume is also a function of wing configuration. Assuming that 80 percent of the wing box contains fuel, figure 20 shows that the fuel volume availability for this vehicle becomes critical at an aspect ratio greater than approximately 29.

PERFORMANCE ANALYSIS

The performance characteristics of the baseline configuration were determined analytically, and then, using a consistent methodology, performance analyses were conducted on the alternate configurations. The various configurations developed in this study were compared assuming a constant cruise at 19.8 km (65 000 ft). The strut-braced configuration exhibiting the maximum cruise range was also compared using the optimum cruise-climb technique. Maximum altitude capability is noted for the baseline concept as well as for two strut-braced configurations. All configurations carry the same payload and fuel for each mission.

Baseline Airplane Performance

The baseline aircraft has significant capability for high-altitude, subsonic flight. It has a nominal operating altitude range of from 19.8 to 21.3 km (65 000 to 70 000 ft) with an absolute ceiling of approximately 23.2 km (76 000 ft). Some of the estimated boundaries of the flight envelope are presented in terms of airspeed and altitude in figure 21. The normal operational airspeed is given as 180 KEAS up to M = 0.69, and the climb speed as 160 KEAS up to M = 0.70.

A normal flight profile is described in reference 1. This profile consists of a climb from sea level to 19.8 km (65 000 ft), a cruise segment maintained at that altitude, and descent to sea level, for a total range of approximately 4.65 km (2500 n.mi.). Calculations of baseline performance were made for a payload of 6.45 kN (1450 lb), 19.8 km (65 000 ft) cruise altitude, and M = 0.69 cruise speed; the results given in table III(a), agree closely with the available data.

Constant Altitude Cruise

The constant-altitude cruise mission assumes a maximum-power climb to 19.8 km (65 000 ft) followed by the cruise segment at M = 0.69, then a descent to sea level at idle thrust with the landing gear extended and the aft fuselage speed-brakes fully deployed. Figure 22 presents a plot of specific range versus Mach number as a function of the baseline aircraft weight at an altitude of 19.8 km (65 000 ft). Although the maximum specific range speed is approximately M = 0.76, the estimated high-speed buffet-limitation line precludes operation at that Mach number. Also presented on this figure is the clean configuration 1g stall limit-line for C_L = 1.1. In order to allow for safe operation in rough air, it has been assumed that the airplane normally cruises at M = 0.69.

Table III presents the mission summary for the four cantilever configurations, all with a wing area of 57.6 m^2 (620 ft^2). The strut-braced equivalent configuration mission capability is also presented in table III. As shown in figure 23, plotting the cruise-segment range versus wing aspect ratio indicated optimum aspect ratios of 26.2 and 28.3 for the cantilever and strut-braced configurations, respectively, with corresponding increases in cruise range of 18.6

and 31.4 percent. Table III also presents the detailed mission summary for the optimum strut-braced configuration with aspect ratio 28.3.

Cruise-Climb

The cruise-climb technique assumes that the aircraft climbs at M = .69 at the peak of the specific range curve as a function of pressure altitude and airplane weight. The resulting cruise-climb maximum specific range versus airplane weight was reduced by one percent to correct for the resulting rate-of-climb of approximately 3.0 m/min (10 ft/min). Table IV presents the mission summary for the strut-braced configuration with a 57.6 m^2 (620 ft^2) aspect ratio 28.3 wing and also a larger wing of 92.9 m^2 (1000 ft^2) with the same aspect ratio. For a cruise initiation altitude of 19.8 km (65 000 ft) and standard wing area, the optimum aspect-ratio, strut-braced configuration gave approximately the same calculated range and endurance for both optimum cruise-climb and constant-altitude cruise (table IV). The optimum altitude for start of the climb-cruise for the large-wing configuration is 21.0 km (69 000 ft). The cruise-climb range of this larger wing configuration is approximately 185.20 km (100 n.mi.) shorter than for the smaller wing concept due to the heavier gross weight and the availability of less cruise fuel (extra fuel to climb to and descend from the higher altitude).

Maximum Altitude Capability

The high aspect-ratio configurations with standard wing areas offered no improvement in absolute ceiling compared to the baseline configuration. The baseline design has an absolute ceiling of 23.2 m (76 100 ft) at 67.2 kN (15 000 lbf); the optimum aspect-ratio, strut-braced configuration was calculated to reach the same altitude, but at 70.4 kN (15 820 lbf). However, to attain this altitude requires 20 degrees of trailing-edge flap deflection because of the larger lift coefficients. For comparison, the strut-braced configuration with the large wing has an absolute ceiling of 25.1 km (82 500 ft) at 80.1 kN (18 000 lbf). This is an 8.2 percent increase.

CONCLUSIONS

A study was conducted to ascertain the effect of high-aspect-ratio strut-braced wings on configuration structural weight, system weight, range, and altitude performance. Performance comparisons were made between jet-powered, high-altitude configurations with cantilever wings and wings with lifting struts. Fuselage and engine characteristics, payload, takeoff fuel weight, and wing area remained the same as for the baseline cantilever design except for one strut-braced configuration with approximately 61 percent more wing area.

1. Strut-braced wings are lighter than cantilever wings, for the same area and aspect ratio, particularly at higher aspect ratios.

2. For constant-altitude cruise with standard-area wings, maximum range was indicated for aspect ratios of 26.2 and 28.3 for the cantilever and strut-braced configurations, respectively. In comparison to the baseline cantilever configuration, with aspect ratio 10.32, these optimum cantilever and strut-braced configurations offer improvements in cruise range of 18.6 and 31.1 percent, respectively.

3. For a cruise initiation altitude of 19.8 km (65 000 ft) and standard wing area, the optimum aspect-ratio, strut-braced configuration gave approximately the same calculated range and endurance for both optimum cruise-climb and constant-altitude cruise.

4. The optimum aspect-ratio, standard wing area, strut-braced configuration is calculated to achieve approximately the same absolute ceiling as the baseline configuration. The strut-braced configuration with larger wing area was calculated to have an 8.2 percent improvement in absolute ceiling without using the large flap deflections required by the standard-area wings.

REFERENCES

1. Anon.: High-Altitude Perspective. NASA SP-427, 1978.

2. DeYoung, John: Wing Loading Theory Satisfying All Boundary Points. Ph.D. Dissertation, Department of Aerospace Engineering, The University of Texas at Arlington, 1975.

3. Hoerner, Sighard F.: Fluid Dynamic Drag. Published by the author, 1958.

4. Dollyhigh, Samuel M.; Monta, William J.; and Sangiorgio, Giuliana: Longitudinal Aerodynamic Characteristics at Mach 0.60 to 2.86 of a Fighter Configuration with Strut Braced Wing. NASA TP-1102, 1977.

5. Jobe, Charles E.; Kulfan, Robert M.; and Vachal, John D.: Wing Planforms for Large Military Transports. Journal of Aircraft, Vol. 16, July 1979, pp. 425-432.

6. Whetstone, W. D.: SPAR Structural Analysis System Reference Manual, System Level 14. NASA CR-145098, 1979.

7. Betz, Albert: Applied Airfoil Theory. Aerodynamic Theory, Vol.IV, Durand, W.F., Editor-in-chief, Julius Springer, Berlin, 1934.

8. Glauert, Hermann: The Elements of Aerofoil and Airscrew Theory, Cambridge University Press, London, 1926.

9. Wood, K. D.: Aerospace Vehicle Design, Volume I, Aircraft Design, Johnson Publishing Company, Boulder, Colorado, 1963.

10. DOT/FAA Airworthiness Standards: Transport Category Airplanes, FAR Part 25, June 1974.

11. Scanlon, Robert H.; and Rosenbaum, Robert: Introduction to the Study of Aircraft Vibration and Flutter, The Macmillan Company, 1951.

TABLE I. - DIMENSIONAL CHARACTERISTICS OF SUBSONIC HIGH-ALTITUDE AIRCRAFT CONFIGURATIONS

(a) Baseline configuration

Wing:		
Area, m^2 (ft^2)	57.600	(620)
Span, m (ft)	24.384	(80)
Aspect ratio		10.32
Mean aerodynamic chord, m (ft)	2.634	(8.643)
Horizontal tail:		
Area, m^2 (ft^2)	9.160	(98.600)
Span, m (ft)	6.239	(20.470)
Aspect ratio		4.25
Mean aerodynamic chord, m (ft)	1.533	(5.028)
Distance from wing 0.25$\bar{c}$ to horizontal-tail 0.25$\bar{c}$, m (ft)	6.337	(20.790)
Vertical tail:		
Area, m^2 (ft^2)	4.041	(43.500)
Span, m (ft)	2.822	(9.257)
Aspect ratio		1.97
Mean aerodynamic chord, m (ft)	1.722	(5.650)
Distance from wing 0.25$\bar{c}$ to vertical-tail 0.25 $\bar{c}$, m (ft)	6.419	(21.060)

TABLE I. - Continued

(b) Strut-braced configuration, A = 20

Wing:		
Area, m^2 (ft^2)	57.600	(620)
Span, m (ft)	33.941	(111.355)
Aspect ratio		20
Mean aerodynamic chord, m (ft)	1.837	(6.026)
Horizontal tail:		
Area, m^2 (ft^2)	9.160	(98.600)
Span, m (ft)	6.239	(20.470)
Aspect ratio		4.25
Mean aerodynamic chord, m (ft)	1.533	(5.028)
Distance from wing 0.25$\bar{c}$ to horizontal-tail 0.25$\bar{c}$, m (ft)	6.337	(20.790)
Vertical tail:		
Area, m^2 (ft^2)	5.625	(60.550)
Span, m (ft)	3.330	(10.926)
Aspect ratio		1.97
Mean aerodynamic chord, m (ft)	1.825	(5.986)
Distance from wing 0.25$\bar{c}$ to vertical-tail 0.25$\bar{c}$, m (ft)	6.419	(21.060)

TABLE I. - Continued

(c) Strut-braced configuration, A = 25

Wing:		
Area, m^2 (ft^2)	57.600	(620)
Span, m (ft)	37.947	(124.499)
Aspect ratio		25
Mean aerodynamic chord, m (ft)	1.643	(5.390)
Horizontal tail:		
Area, m^2 (ft^2)	9.160	(98.600)
Span, m (ft)	6.239	(20.470)
Aspect ratio		4.25
Mean aerodynamic chord, m (ft)	1.533	(5.028)
Distance from wing 0.25$\bar{c}$ to horizontal-tail 0.25$\bar{c}$, m (ft)	6.337	(20.790)
Vertical tail:		
Area, m^2 (ft^2)	6.290	(67.700)
Span, m (ft)	3.520	(11.549)
Aspect ratio		1.97
Mean aerodynamic chord, m (ft)	1.929	(6.328)
Distance from wing 0.25$\bar{c}$ to vertical-tail 0.25$\bar{c}$, m (ft)	6.419	(21.060)

TABLE I. - Concluded

(d) Strut-braced configuration, A = 30

Wing:		
Area, m^2 (ft^2)	57.600	(620)
Span, m (ft)	41.569	(136.382)
Aspect ratio		30
Mean aerodynamic chord, m (ft)	1.500	(4.920)
Horizontal tail:		
Area, m^2 (ft^2)	9.160	(98.600)
Span, m (ft)	6.239	(20.470)
Aspect ratio		4.25
Mean aerodynamic chord, m (ft)	1.533	(5.028)
Distance from wing 0.25$\bar{c}$ to horizontal-tail 0.25$\bar{c}$, m (ft)	6.337	(20.790)
Vertical tail:		
Area, m^2 (ft^2)	6.890	(74.160)
Span, m (ft)	3.685	(12.090)
Aspect ratio		1.97
Mean aerodynamic chord, m (ft)	2.019	(6.625)
Distance from wing 0.25$\bar{c}$ to vertical-tail 0.25$\bar{c}$, m (ft)	6.419	(21.060)

TABLE II. - ESTIMATED VEHICLE WEIGHTS

(a) Cantilever configuration, S = 57.600 m^2 (620 ft^2)

Wing aspect ratio	10.32		20		25		30	
	kN	lbf	kN	lbf	kN	lbf	kN	lbf
Structure - excluding wing	10.9	2450	11.1	2490	11.3	2550	11.6	2610
- wing	12.5	2810	16.3	3670	20.6	4630	25.3	5680
Propulsion	24.1	5420	24.1	5420	24.1	5420	24.1	5420
Systems	6.1	1380	6.5	1470	6.7	1510	6.9	1560
Weight Empty	53.6	12060	58.0	13050	62.7	14110	67.9	15270
Operating Items	1.6	350	1.6	350	1.6	350	1.6	350
Operating Weight Empty	55.2	12410	59.6	13400	64.3	14460	69.5	15620
Payload	6.5	1450	6.5	1450	6.5	1450	6.5	1450
Zero Fuel Weight	61.7	13860	66.1	14850	70.8	15910	75.9	17070
Mission Fuel	32.5	7300	32.5	7300	32.5	7300	32.5	7300
Take-off Gross Weight	94.1	21160	98.5	22150	103.2	23210	108.4	24370

TABLE II. - Continued

(b) Strut-braced configuration, η_s = .4

Wing aspect ratio	10.32		20		25		30	
	kN	lbf	kN	lbf	kN	lbf	kN	lbf
Structure - excluding wing	10.8	2420	10.8	2430	10.9	2450	11.1	2490
- wing	10.9	2460	11.8	2660	13.4	3020	15.9	3580
Propulsion	24.1	5420	24.1	5420	24.1	5420	24.1	5420
Systems	6.1	1380	6.4	1430	6.5	1460	6.6	1490
Weight Empty	52.0	11680	53.1	11940	54.9	12350	57.7	12980
Operating Items	1.6	350	1.6	350	1.6	350	1.6	350
Operating Weight Empty	53.5	12030	54.7	12290	56.5	12700	59.3	13330
Payload	6.5	1450	6.5	1450	6.5	1450	6.5	1450
Zero Fuel Weight	60.0	13480	61.1	13740	62.9	14150	65.7	14780
Mission Fuel	32.5	7300	32.5	7300	32.5	7300	32.5	7300
Take-off Gross Weight	92.4	20780	93.6	21040	95.4	21450	98.2	22080

TABLE II. - Concluded

(c) Strut-braced configuration, n_s = .4, S = 92.903 m^2 (1000 ft^2)

Wing aspect ratio	28.3	
	kN	lbf
Structure - excluding wing	11.6	2600
- wing	23.8	5340
Propulsion	24.1	5420
Systems	7.0	1580
Weight Empty	66.5	14940
Operating Items	1.6	350
Operating Weight Empty	68.0	15290
Payload	6.5	1450
Zero Fuel Weight	74.5	16740
Mission Fuel	32.5	7300
Take-off Gross Weight	106.9	24040

TABLE III. - MISSION RANGE CAPABILITY FOR CRUISE AT M = 0.69 AND CONSTANT ALTITUDE

(a) Cantilever configuration, S = 57.600 m^2(620 ft^2)

Configuration	Baseline, wing aspect ratio = 10.32				Wing aspect ratio = 20			
	Operating Weight kN lbf	Fuel kN lbf	Range Mm n.mi.	Time min	Operating Weight kN lbf	Fuel kN lbf	Range Mm n.mi	Time min
Depart ramp	94.124 (21 160)				98.506 (22 145)			
		.262 (59)	0 0	0		.262 (59)	0 0	0
Takeoff	93.872 (21 101)				98.243 (22 086)			
		2.366 (532)	0 0	2		2.366 (532)	0 0	2
Start Climb	91.495 (20 569)				95.877 (21 554)			
		5.222 (1 174)	.137 (74)	12		5.387 (1 211)	137 (74)	12
Start cruise at 19.812 km (65 000 ft)	86.273 (19 395)				90.490 (20 343)			
		20.253 (4 553)	4.254 (2 297)	348		20.035 (4 504)	4.871 (2 630)	399
End Cruise at 19.812 km (65 000 ft)	66.021 (14 842)				70.455 (15 839)			
		1.455 (327)	.265 (143)	29		1.508 (339)	.274 (148)	30
End descent	64.566 (14 515)				68.947 (15 500)			
	Σ	29.558 (6 645)	4.656 (2 514)	391	Σ	29.558 (6 645)	5.282 (2 852)	443
	Fuel reserves	2.914 (655); 378.5 liters (100 U.S. gal)			Fuel reserves	2.914 (655); 378.5 liters (100 U.S. gal)		
	Max. fuel	32.472 (7 300)			Max. fuel	32.472 (7 300)		

TABLE III. - Continued

(a) Concluded

Configuration	Wing aspect ratio = 25				Wing aspect ratio = 30			
	Operating weight kN lbf	Fuel kN lbf	Range Mm n.mi.	Time min	Operating weight kN lbf	Fuel kN lbf	Range Mm n.mi.	Time min
Depart ramp	103.243 (23 210)	.262 (59)	0 0	0	108.403 (24 370)	.262 (59)	0 0	0
Takeoff	102.981 (23 151)	2.366 (532)	0 0	2	108.141 (24 311)	2.366 (532)	0 0	2
Start Climb	100.614 (22 619)	5.502 (1 237)	.139 (75)	12	105.774 (23 779)	5.600 (1 259)	.143 (77)	12
Start cruise at 19.812 km (65 000 ft)	95.112 (21 382)	19.852 (4 463)	5.052 (2 728)	414	100.174 (22 520)	19.674 (4 423)	4.954 (2 675)	406
End Cruise at 19.812 km (65 000 ft)	75.259 (16 919)	1.575 (354)	.287 (155)	31	80.499 (18 097)	1.655 (372)	.302 (163)	33
End descent	73.685 (16 565)				78.845 (17 725)			
	Σ	29.558 (6 645)	5.478 (2 958)	459	Σ	29.558 (6 645)	5.399 (2 915)	453
	Fuel reserves	2.914 (655); 378.5 liters (100 U.S. gal)			Fuel reserves	2.914 (655); 378.5 liters (100 U.S. gal)		
	Max. fuel	32.472 (7 300)			Max. fuel	32.472 (7 300)		

TABLE III. - Continued

(b) Strut-braced configuration

Configuration	Wing aspect ratio = 10.32					Wing aspect ratio = 20				
	Operating Weight kN lbf	Fuel kN lbf	Range Mm n.mi.	Time min		Operating Weight kN lbf	Fuel kN lbf	Range Mm n.mi.	Time min	
Depart ramp	92.434 (20 780)	.262 (59)	0 0	0		93.613 (21 045)	.262 (59)	0 0	0	
Takeoff	92.172 (20 721)	2.366 (532)	0 0	2		93.350 (20 986)	2.366 (532)	0 0	2	
Start climb	89.805 (20 189)	5.187 (1 166)	.137 (74)	12		90.984 (20 454)	5.173 (1 163)	.130 (70)	11	
Start cruise at 19.812 km (65 000 ft)	84.619 (19 023)	20.239 (4 550)	4.415 (2 384)	361		85.811 (19 291)	20.226 (4 547)	5.291 (2 857)	433	
End cruise at 19.812 km (65 000 ft)	64.379 (14 473)	1.503 (338)	.265 (143)	29		65.585 (14 744)	1.530 (344)	.270 (146)	29	
End descent	62.876 (14 135)					64.054 (14 400)				
	Σ	29.558 (6 645)	4.817 (2 601)	404		Σ	29.558 (6 645)	5.691 (3 073)	475	
	Fuel reserves	2.914 (655); 378.5 liters (100 U.S. gal)				Fuel reserves	2.914 (655); 378.5 liters (100 U.S. gal)			
	Max. fuel	32.472 (7 300)				Max. fuel	32.472 (7 300)			

TABLE III. - Continued

(b) Concluded

Configuration	Wing aspect ratio = 25					Wing aspect ratio = 30				
	Operating Weight kN lbf	Fuel kN lbf	Range Mm n.mi.	Time min		Operating Weight kN lbf	Fuel kN lbf	Range Mm n.mi.	Time min	
Depart ramp	95.437 (21 455)					98.239 (22 085)				
		.262 (59)	0 0	0			.262 (59)	0 0	0	
Takeoff	95.174 (21 396)					97.977 (22 026)				
		2.366 (532)	0 0	2			2.366 (532)	0 0	2	
Start climb	92.808 (20 864)					95.610 (21 494)				
		5.218 (1 173)	.130 (70)	11			5.249 (1 180)	.131 (71)	11	
Start Cruise at 19,812 km (65 000 ft)	87.590 (19 691)					90.361 (20 314)				
		20.150 (4 530)	5.532 (2 987)	453			20.075 (4 513)	5.565 (3 005)	456	
End cruise at 19.812 km (65 000 ft)	67.439 (15 161)					70.286 (15 801)				
		1.561 (351)	.274 (148)	30			1.606 (361)	.283 (153)	31	
End descent	65.878 (14 810)					68.681 (15 440)				
	Σ	29.558 (6 645)	5.936 (3 205)	496		Σ	29.558 (6 645)	5.980 (3 229)	500	
	Fuel reserves	2.914 (655); 378.5 liters (100 U.S. gal)				Fuel reserves	2.914 (655); 378.5 liters (100 U.S. gal)			
	Max. fuel	32.472 (7 300)				Max. fuel	32.472 (7 300)			

TABLE III. - Concluded

(c) Optimum strut-braced configuration

Configuration	Wing aspect ratio = 28.3			
	Operating Weight kN lbf	Fuel kN lbf	Range Mm n.mi.	Time min
Depart ramp	97.105 (21 830)			
		.262 (59)	0 0	0
Takeoff	96.842 (21 771)			
		2.366 (532)	0 0	2
Start climb	94.476 (21 239)			
		5.240 (1 178)	.131 (71)	11
Start cruise at 19.812 km (65 000 ft)	89.236 (20 061)			
		20.102 (4 519)	5.589 (3 018)	455
End cruise at 19.812 km (65 000 ft)	69.134 (15 542)			
		1.588 (357)	.280 (151)	31
End descent	67.546 (15 185)			
	Σ	29.558 (6 645)	6.000 (3 240)	499
	Fuel reserves	2.914 (655); 378.5 liters (100 U.S. gal)		
	Max. fuel	32.472 (7 300)		

TABLE IV . - MISSION RANGE CAPABILITY FOR OPTIMUM CRUISE-CLIMB AT M = 0.69

(a) Strut-braced configuration, A = 28.3; S = 57.600 m^2 (620 ft^2)

	Operating Weight kN lbf	Fuel kN lbf	Range Mm n.mi.	Time min
Depart ramp	97.105 (21 830)			
		.262 (59)	0 0	0
Takeoff	96.842 (21 771)			
		2.366 (532)	0 0	2
Start Climb	94.476 (21 239)			
		5.240 (1 178)	.131 (71)	11
Start cruise at 19.812 km (65 000 ft)	89.236 (20 061)			
		19.799 (4 451)	5.560 (3 002)	455
End cruise at 20.848 km (68 400 ft)	69.437 (15 610)			
		1.890 (425)	.365 (197)	38
End descent	67.546 (15 185)			
	Σ	29.558 (6 645)	6.056 (3 270)	506
	Fuel reserves	2.914 (655); 378.5 liters (100 U.S. gal)		
	Max. fuel	32.472 (7 300)		

TABLE IV . - Concluded

(b) $S = 92.903\ m^2$ $(1000\ ft^2)$

	Operating Weight kN lbf	Fuel kN lbf	Range Mm n.mi.	Time min
Depart ramp	106.935 (24 040)			
		.262 (59)	0 0	0
Takeoff	106.673 (23 981)			
		2.366 (532)	0 0	2
Start climb	104.306 (23 449)			
		6.463 (1 453)	.183 (99)	17
Start cruise at 21.031 km (69 000 ft)	97.843 (21 996)			
		18.287 (4 111)	5.365 (2 897)	433
End cruise at 22.174 km (72 750 ft)	79.556 (17 885)			
		2.180 (490)	.441 (238)	44
End descent	77.377 (17 395)			
	Σ	29.558 (6 645)	5.989 (3 234)	496
	Fuel reserves	2.914 (655); 378.5 liters (100 U.S. gal)		
	Max. fuel	32.472 (7 300)		

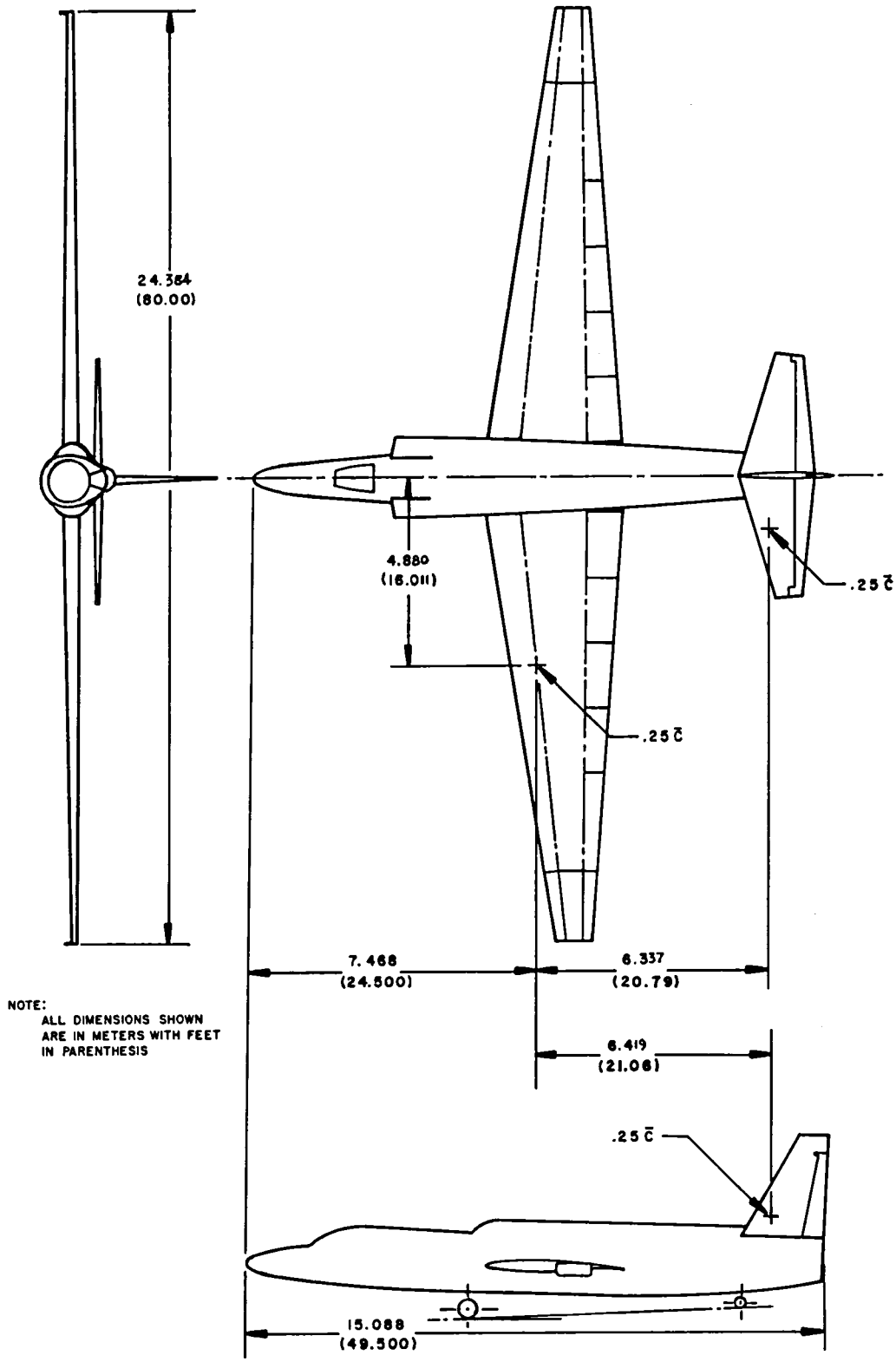

Figure 1. - General arrangement of baseline configuration.

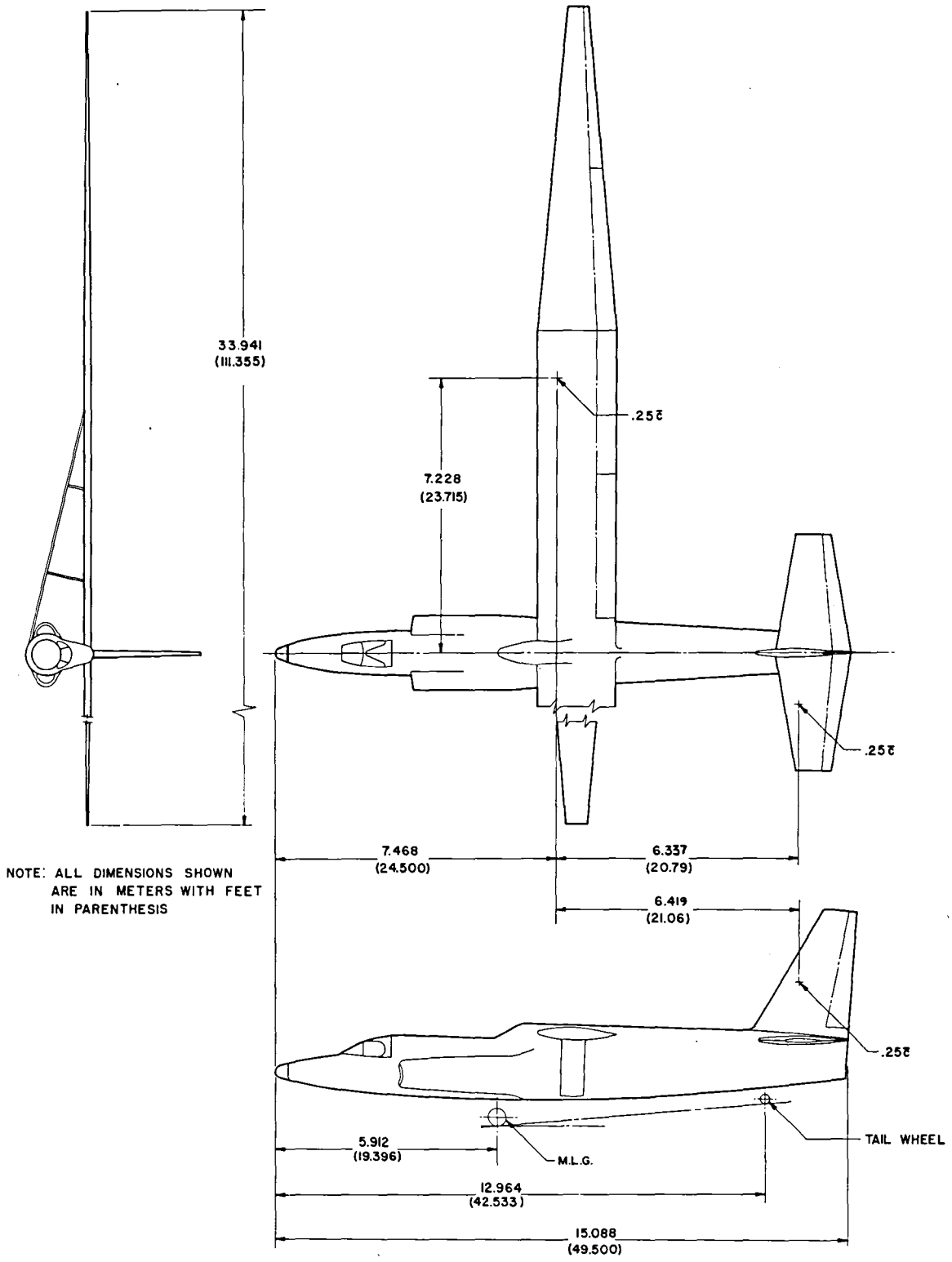

Figure 2. - General arrangement of a typical strutted configuration, aspect ratio = 20.

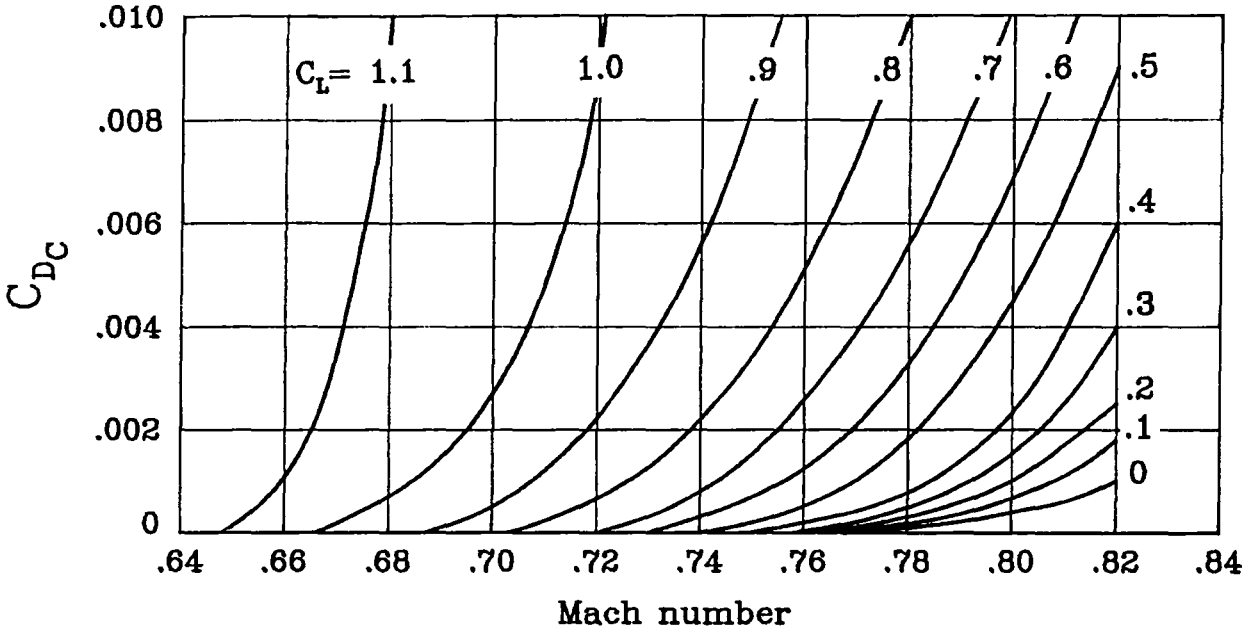

Figure 3. - Estimated compressibility drag, assumed wing thickness-chord ratio = .09.

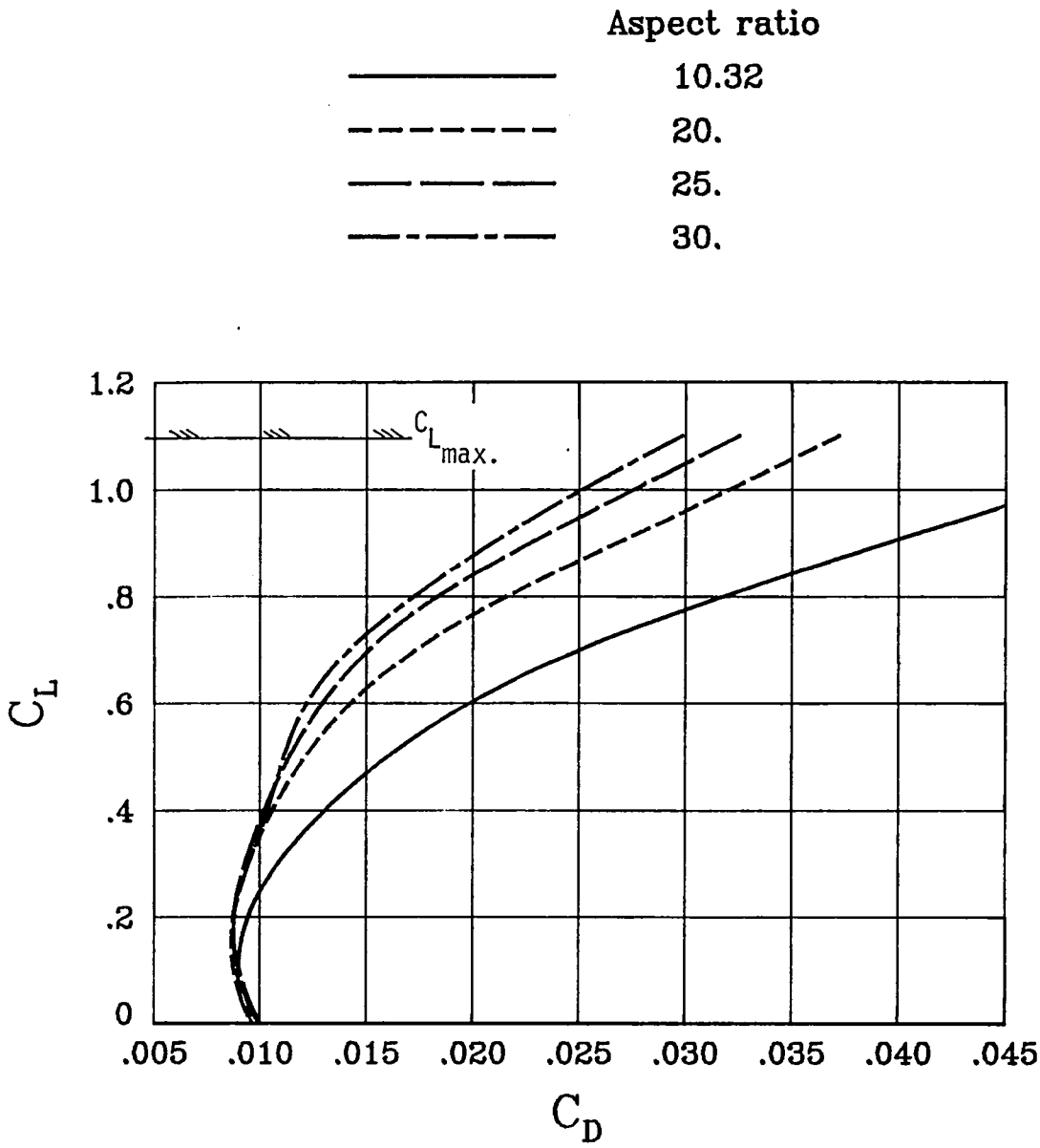

Figure 4. - Estimated lift-drag polar for cantilever wing configurations. Reynolds number based on M = .70 at 12.2 km (40 000 ft), no compressibility drag included. S = 57.6 m^2 (620 ft^2), δ_f = 0°. Speed-brake and landing gear D/q = 1.2 m^2(12.97 ft^2).

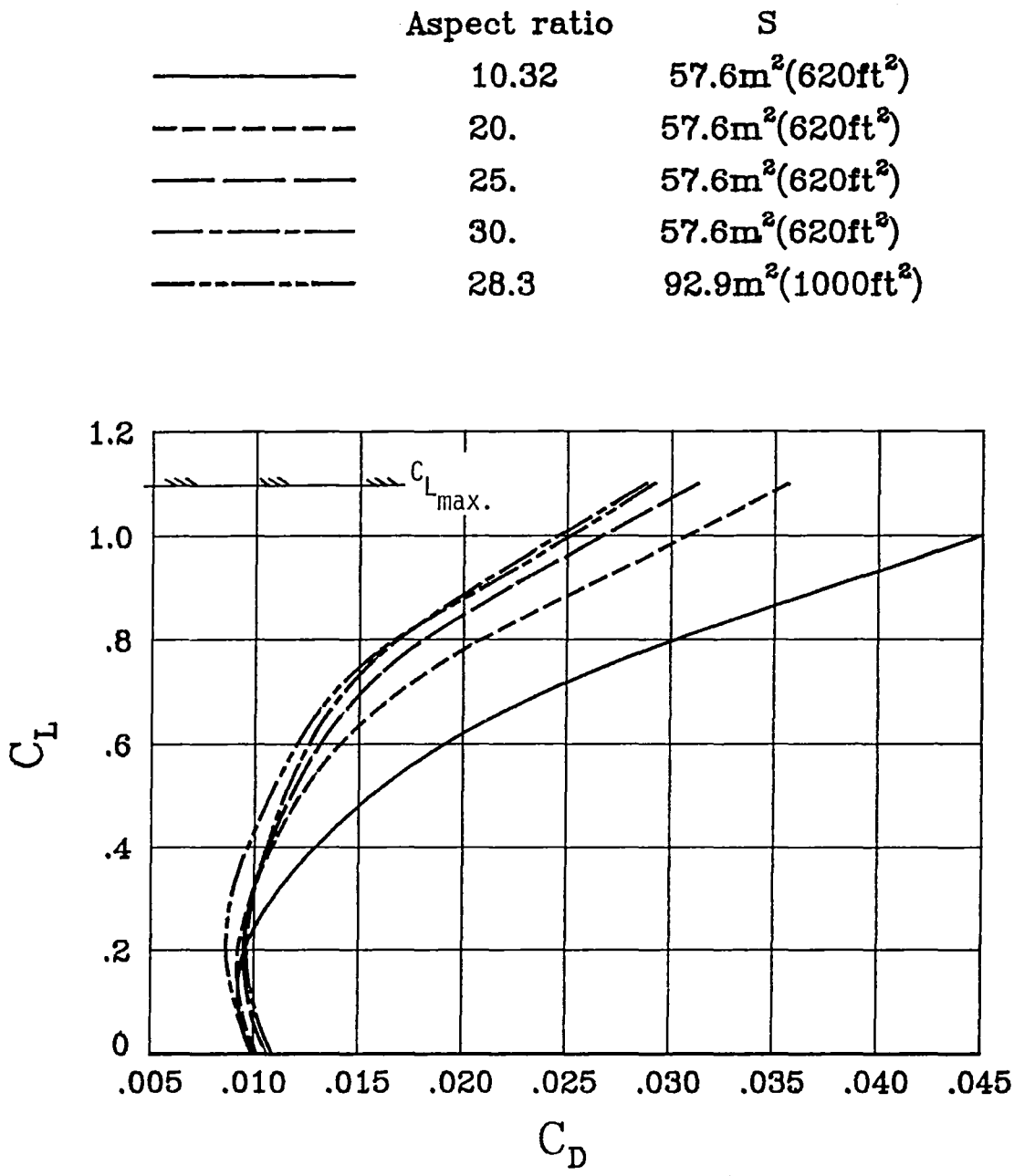

Figure 5. - Estimated lift-drag polars for strut-braced wing configurations. Reynolds number based on M = .70 at 12.2 km (40 000 ft), no compressibility drag included, $\delta_f = 0°$.

Speed-brake and landing gear D/q = 1.2 m^2(12.97 ft^2).

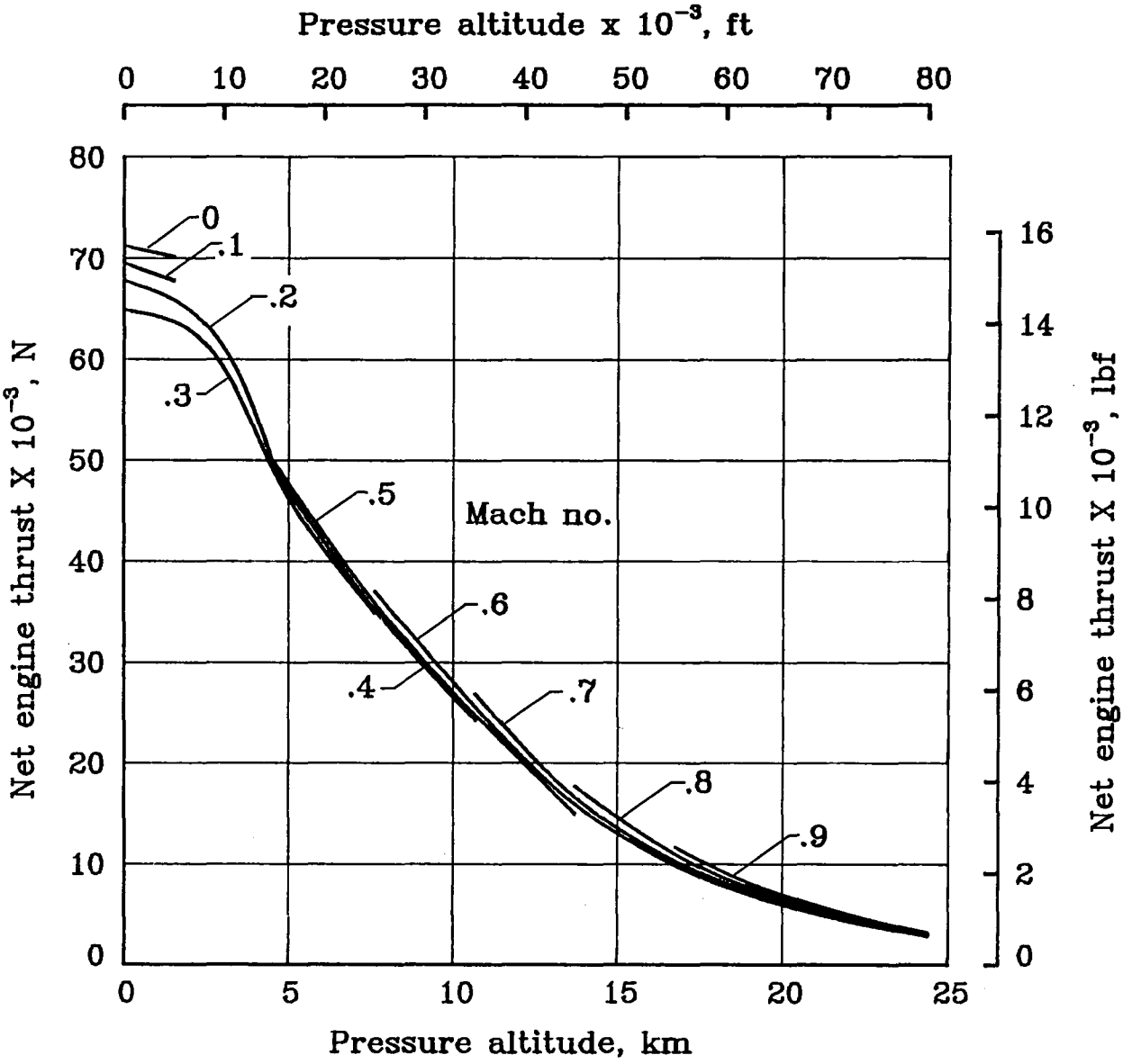

Figure 6. - Estimated installed thrust for maximum climb rating, standard day atmospheric conditions.

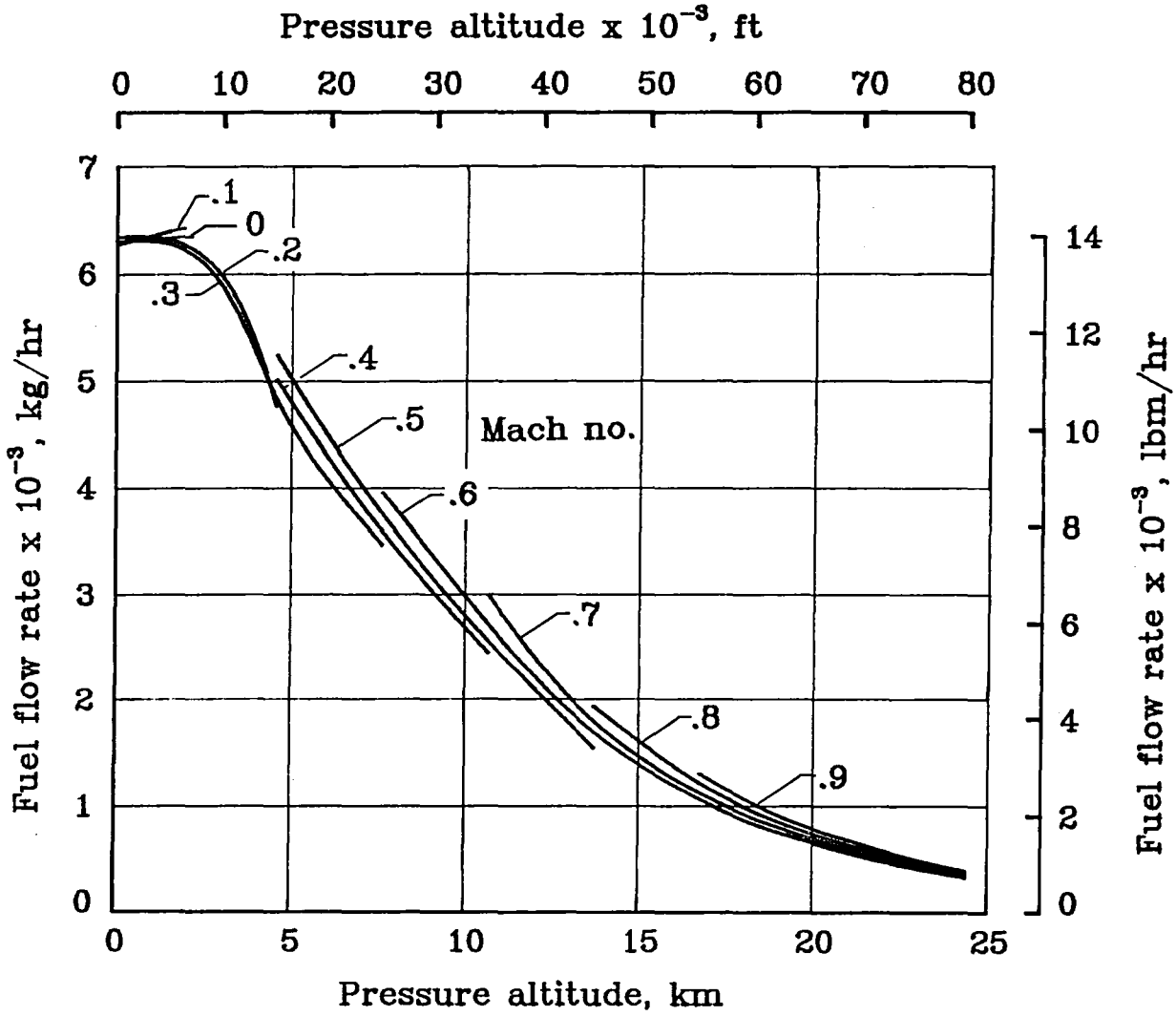

Figure 7. - Estimated installed fuel flow rate for maximum climb rating, standard day atmospheric conditions.

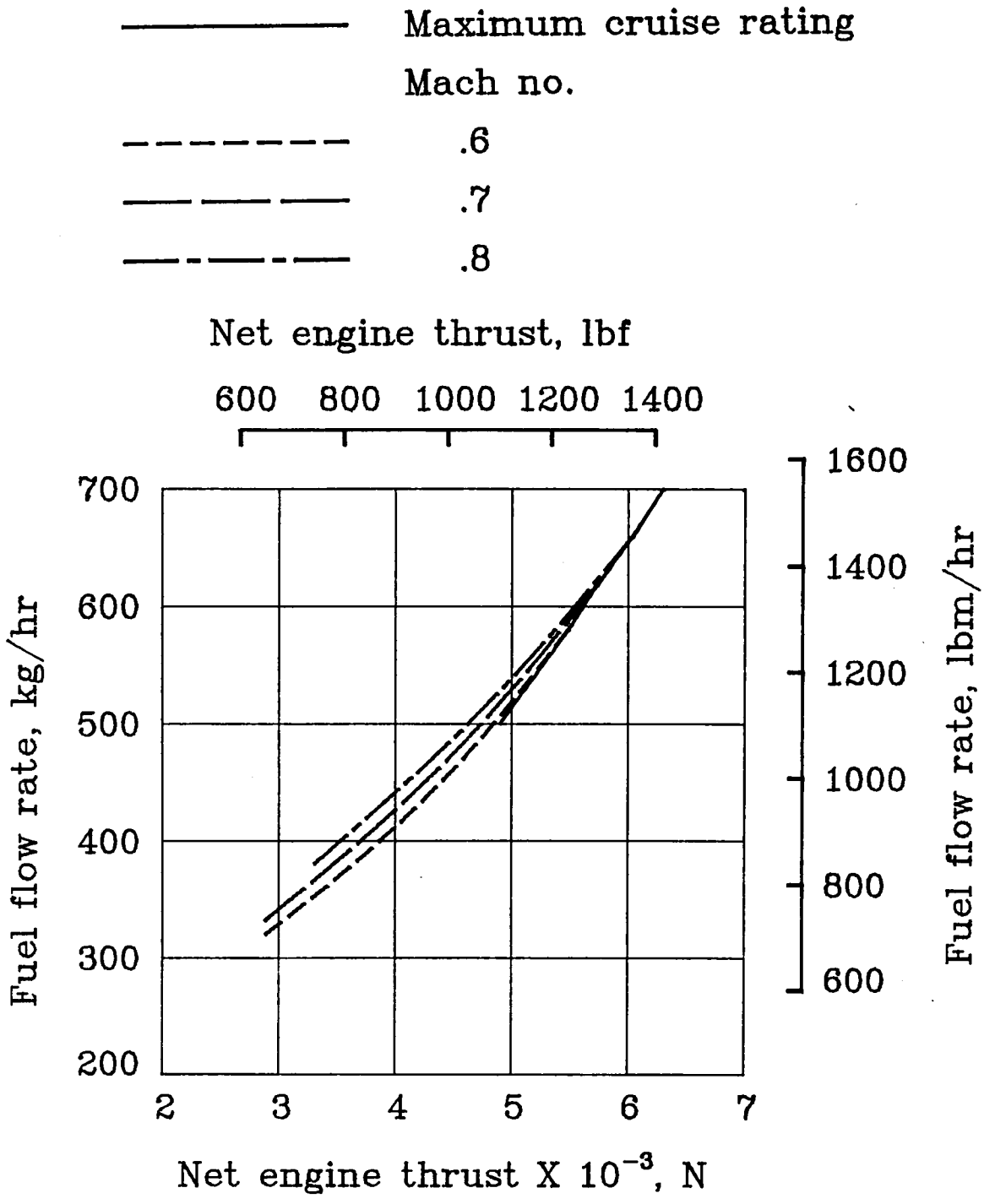

(a) Pressure altitude, 19.8 km (65 000 ft)

Figure 8. - Estimated installed thrust and fuel flow rate for maximum and part power cruise, standard day atmospheric conditions.

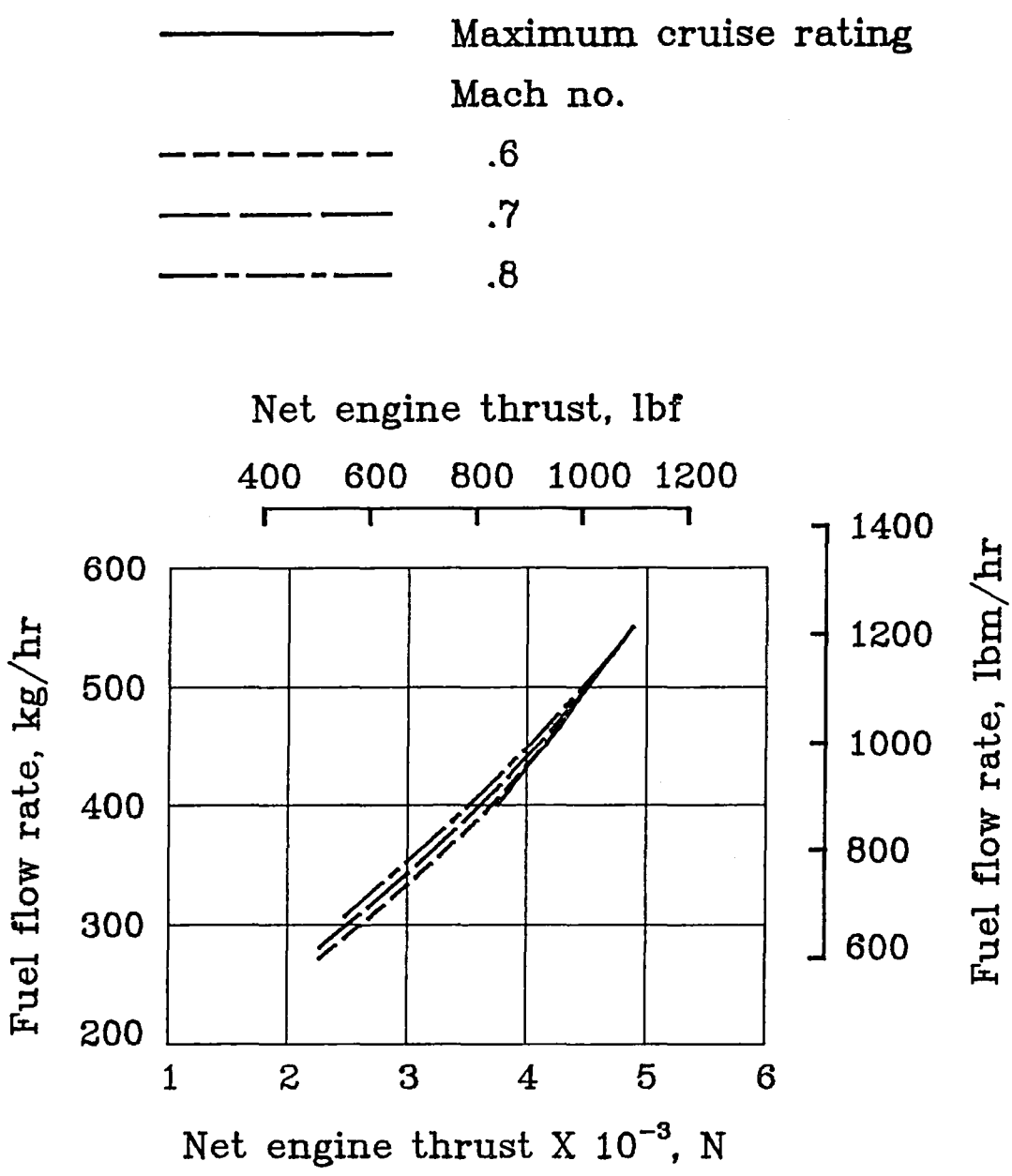

(b) Pressure altitude, 21.3 km (70 000 ft)

Figure 8. - Continued.

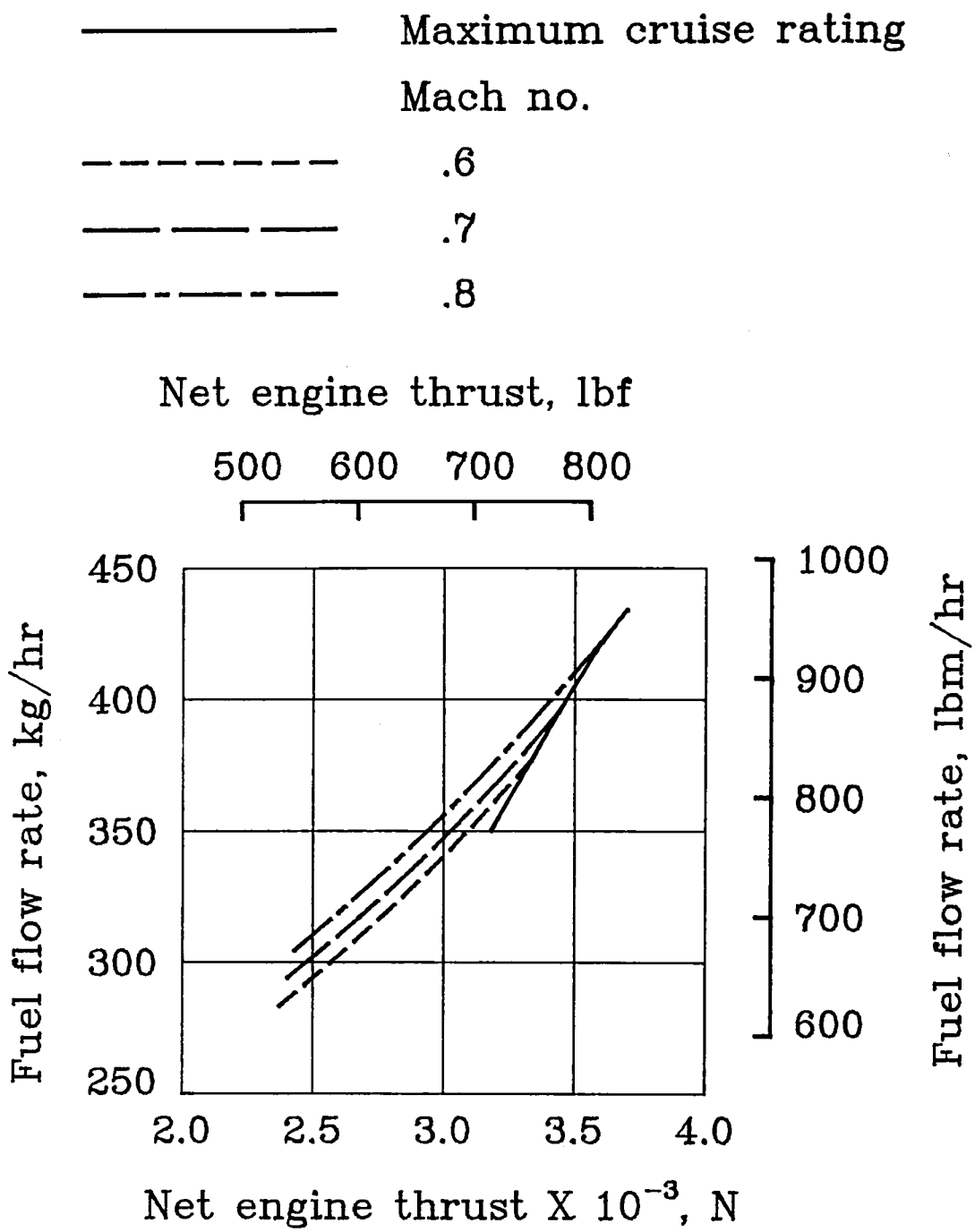

(c) Pressure altitude, 22.9 km (75 000 ft)

Figure 8. - Continued.

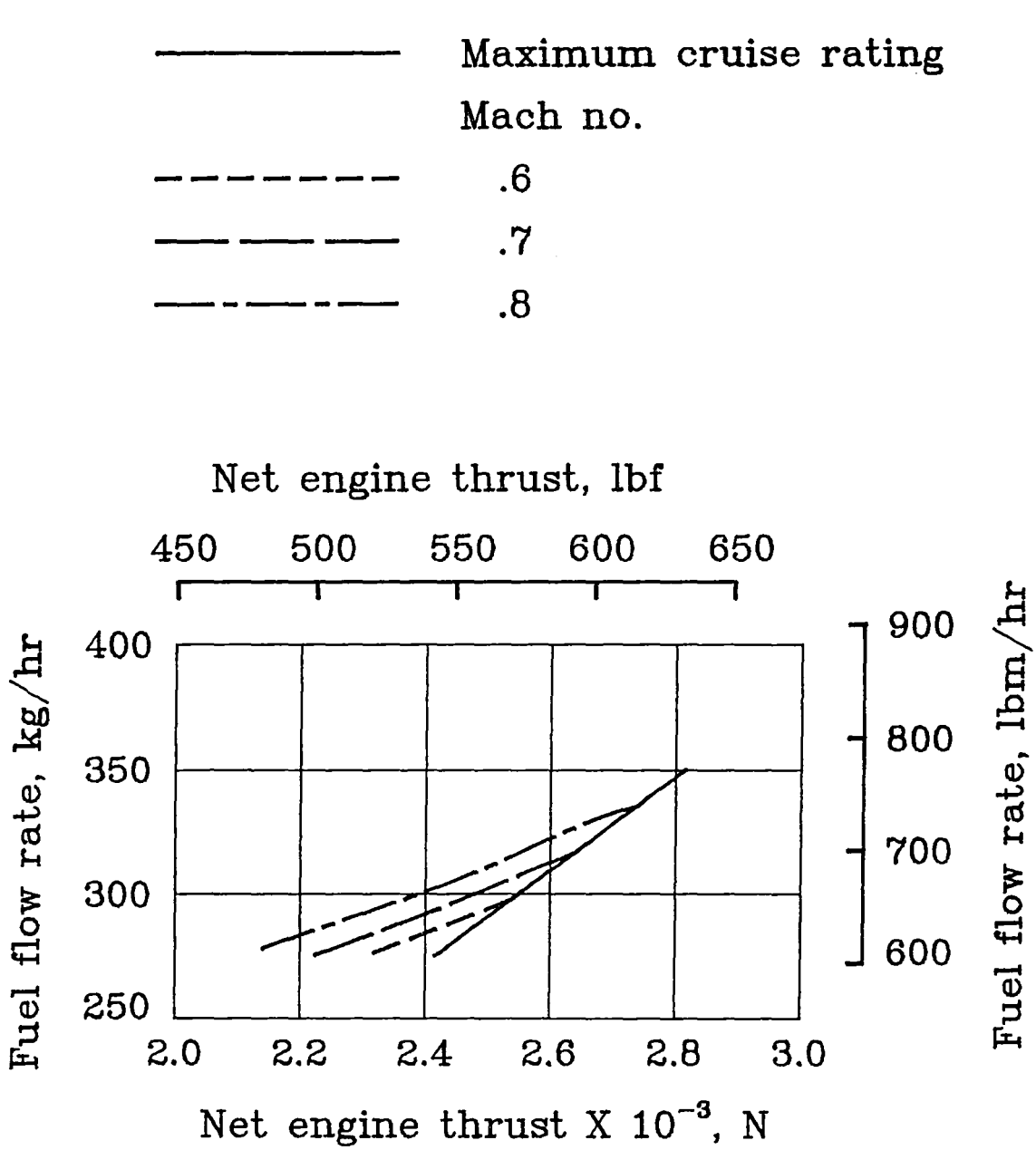

(d) Pressure altitude, 24.4 km (80 000 ft)

Figure 8. - Concluded.

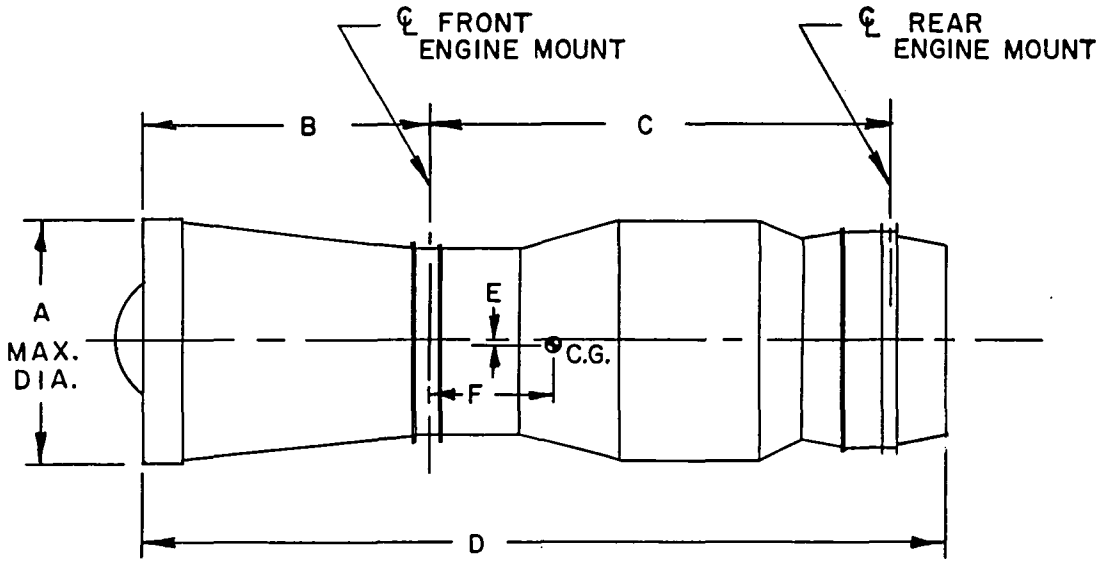

DIMENSION	METERS	INCHES
A	1.09	43.0
B	1.27	50.0
C	2.08	82.0
D	3.73	147.0
E	.03	1.0
F	.56	22.0

Figure 9. - High-altitude turbojet engine overall dimensions.

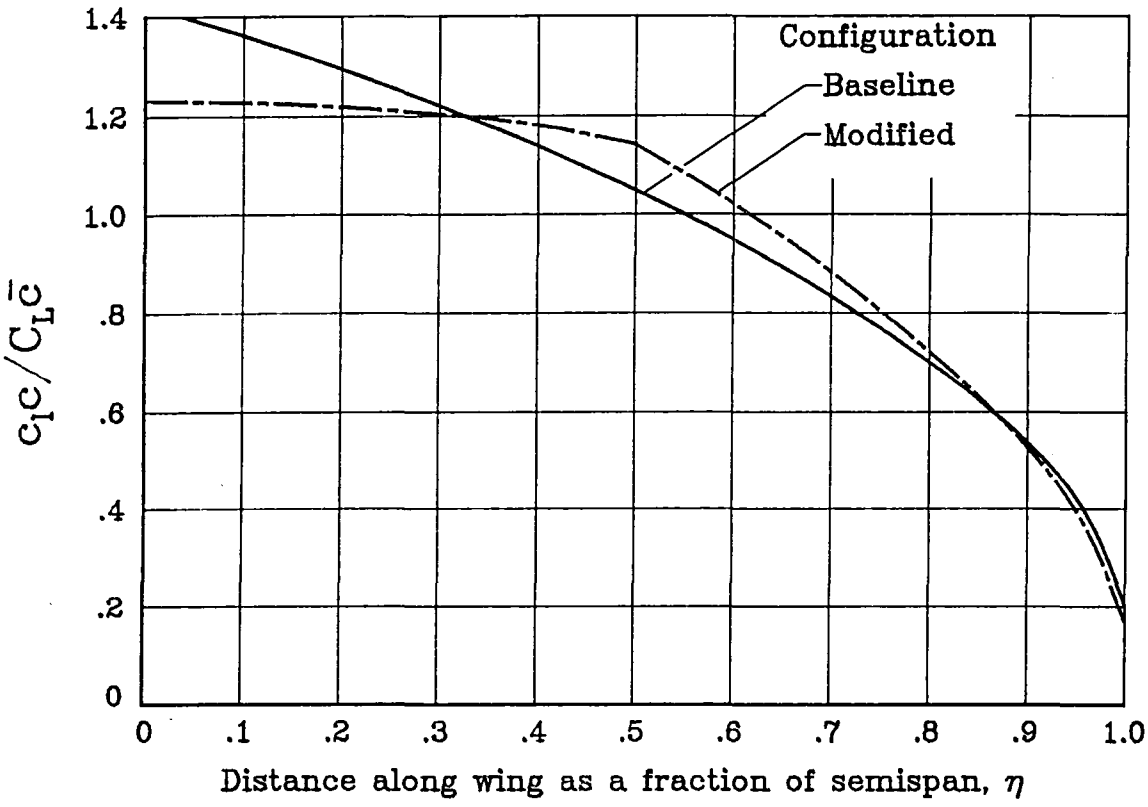

Figure 10.- Estimated wing unit-span-load distribution.

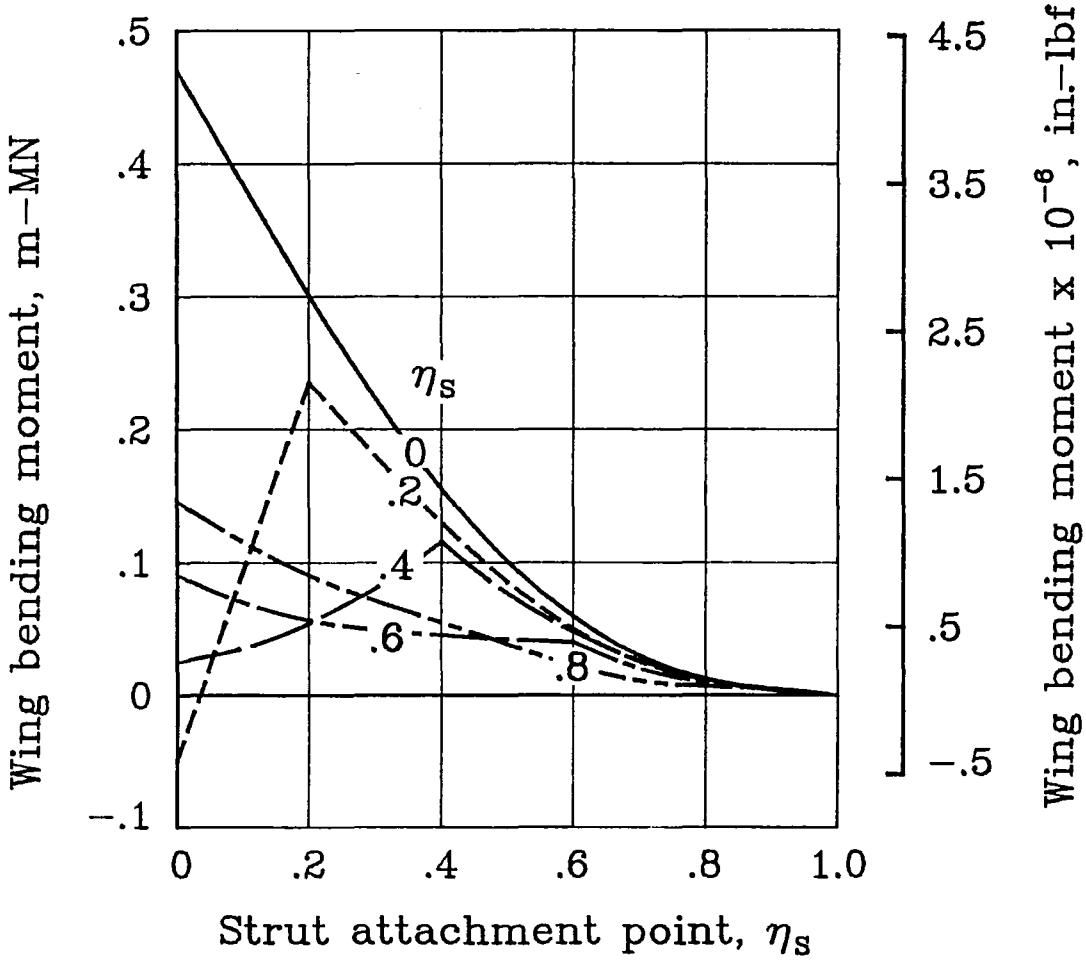

Figure 11. - Estimated wing bending moment, A = 25; 94 percent full fuel condition, +2g maneuver limit load, S = 57.6 m^2 (620 ft^2).

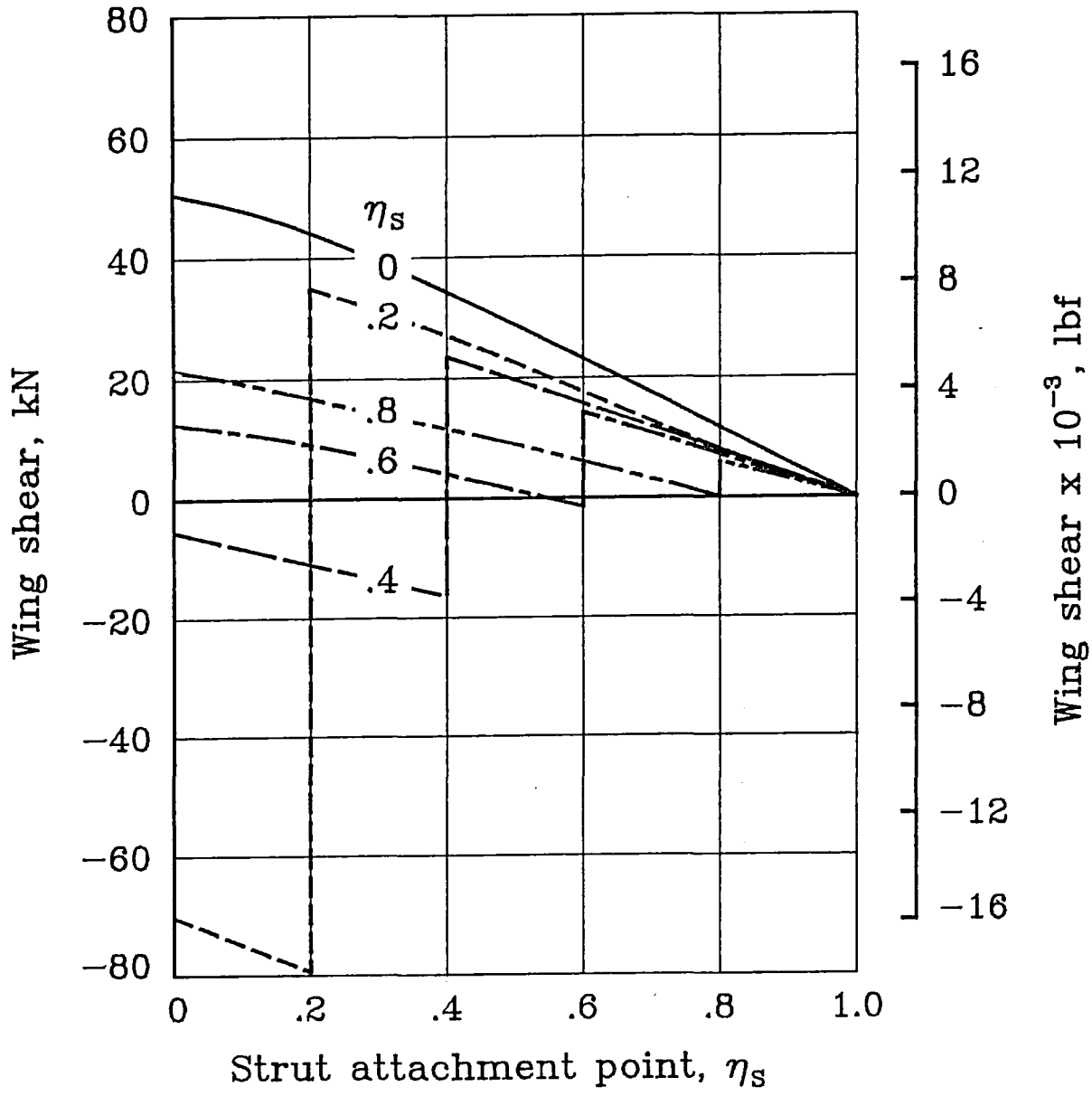

Figure 12. - Estimated wing shear force, A = 25 ; 94 percent full fuel condition, +2g maneuver limit load, S = 57.6 m^2 (620 ft^2).

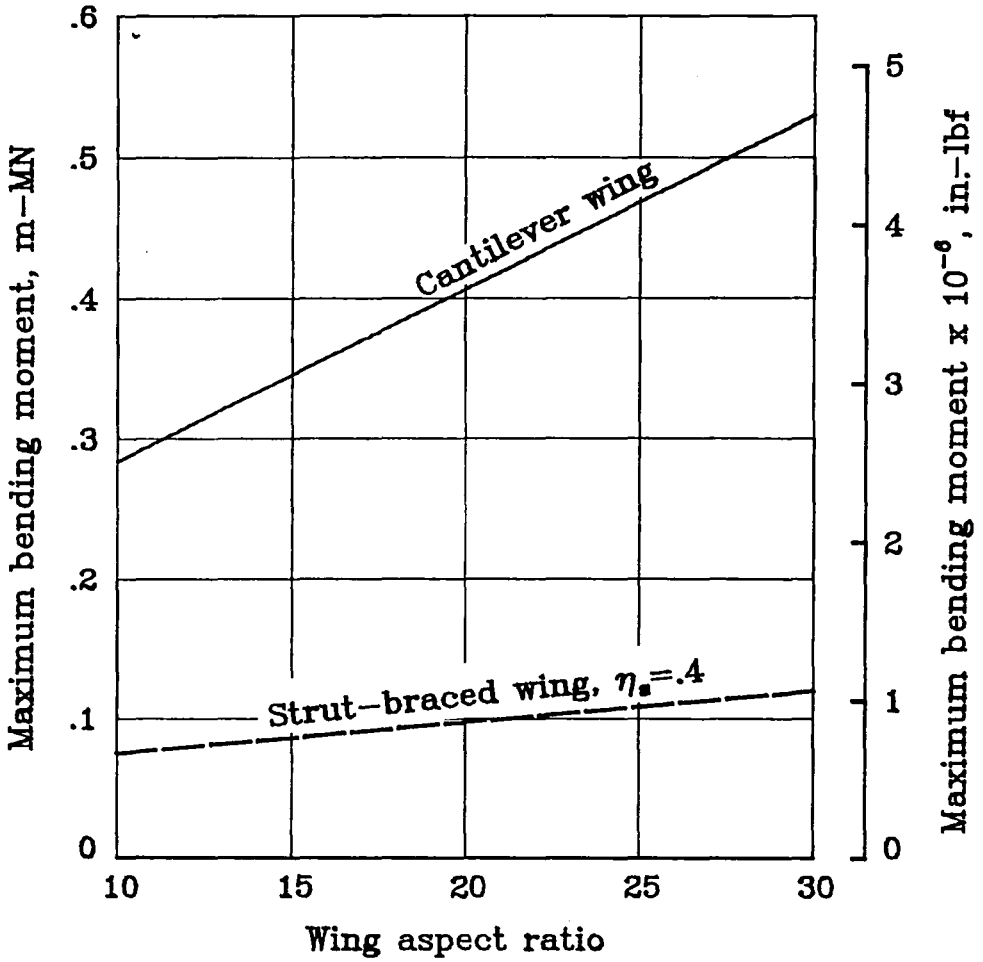

Figure 13. - Estimated maximum wing bending moments ; 94 percent full fuel condition, +2g maneuver limit load, S = 57.6 m^2 (620 ft^2).

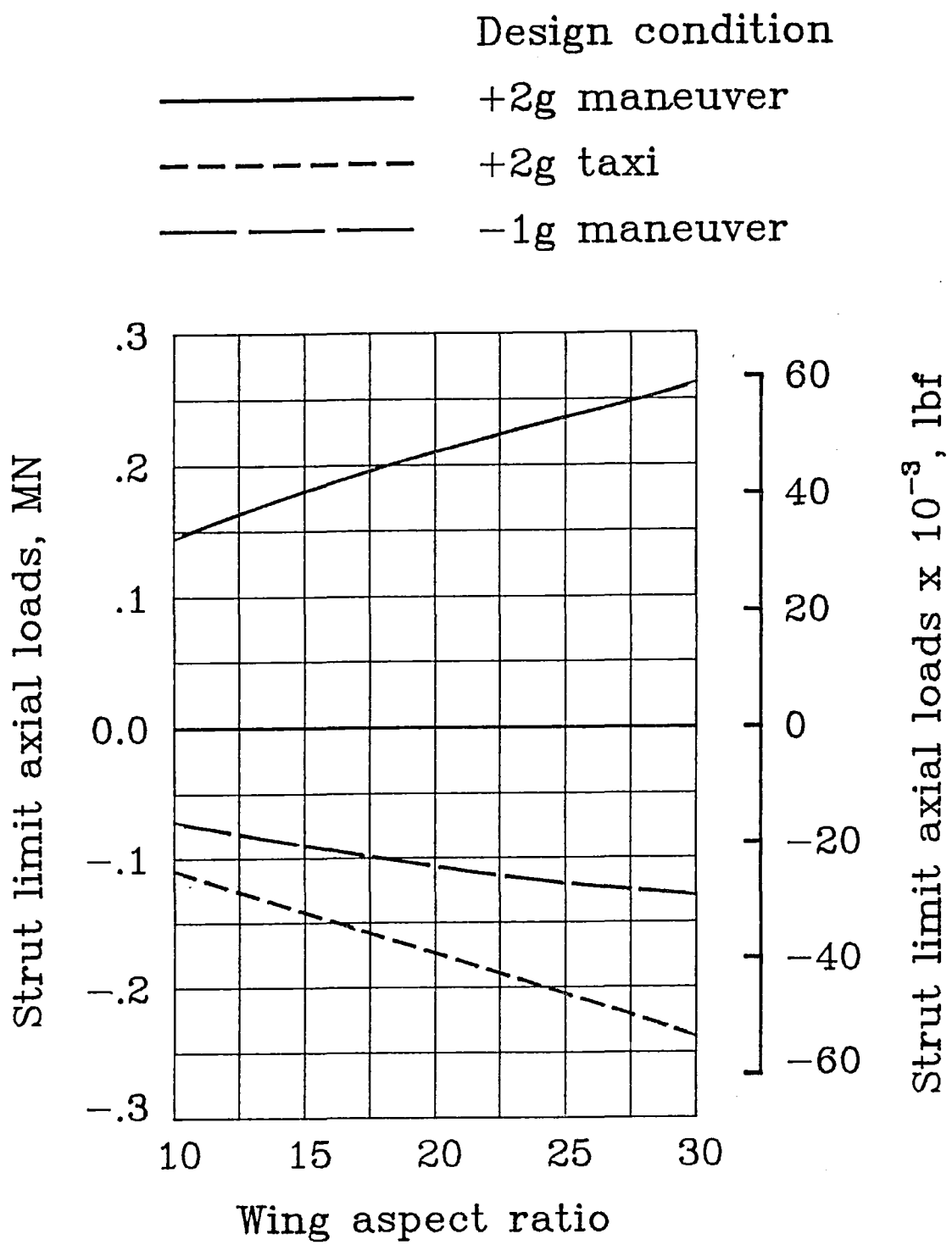

Figure 14. - Estimated strut axial loads ; 94 percent full fuel condition, S = 57.6 m^2 (620 ft^2).

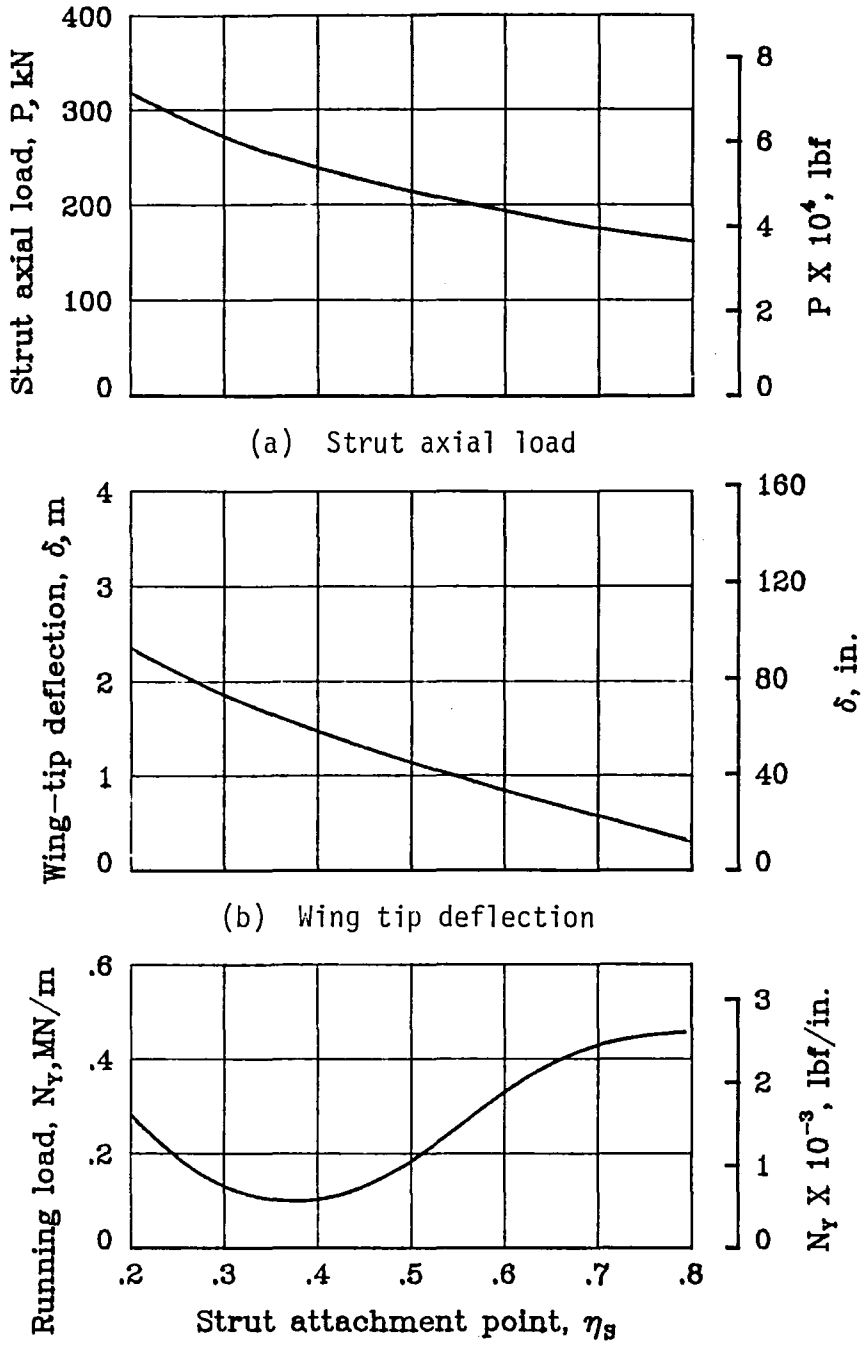

Figure 15. - Estimated strut-braced wing structural characteristics, A = 25; 94 percent full fuel condition, +2g maneuver limit load, S = 57.6 m^2 (620 ft^2).

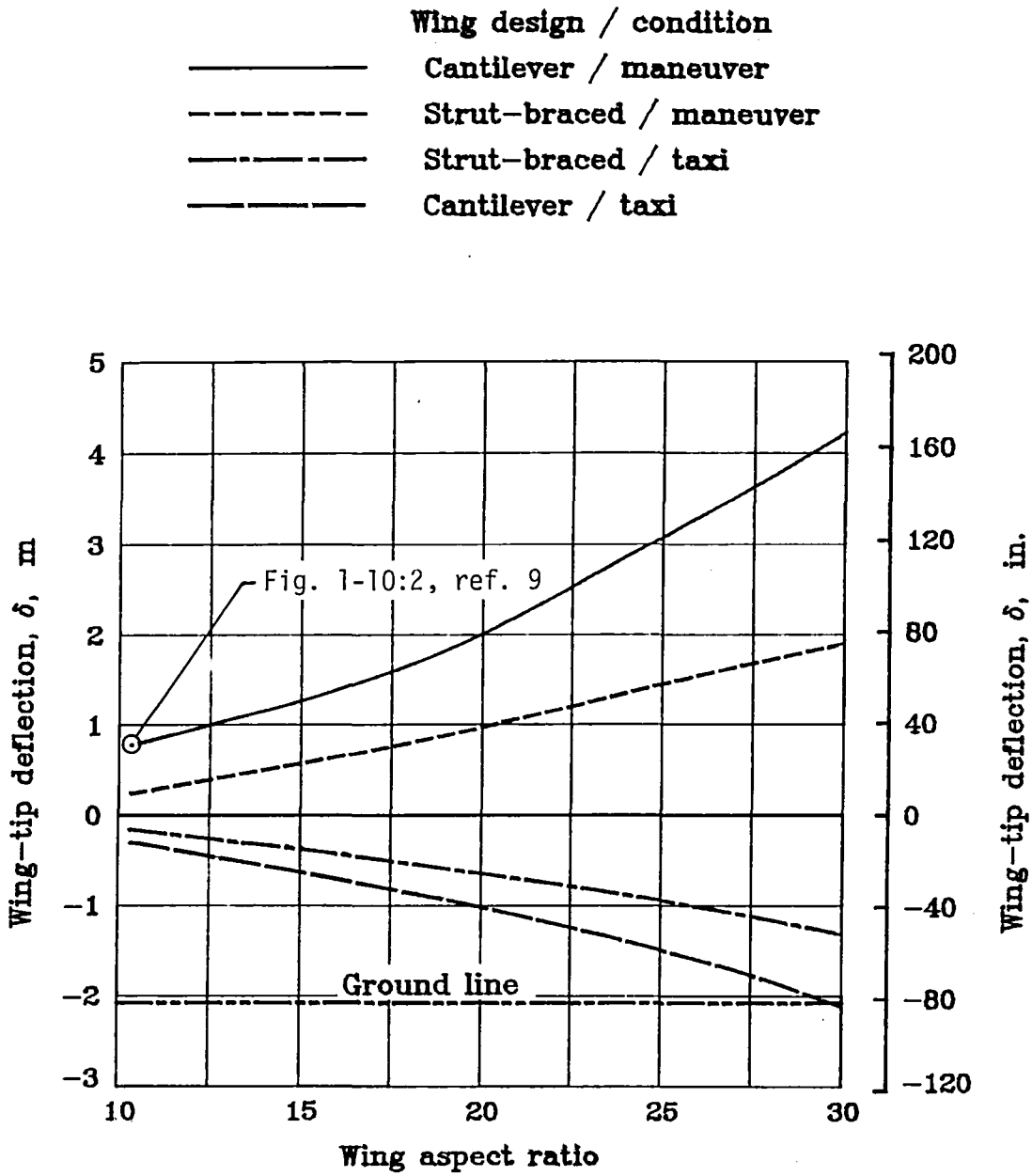

Figure 16. - Estimated wing tip deflections ; 94 percent full fuel conditions, S = 57.6 m^2 (620 ft^2).

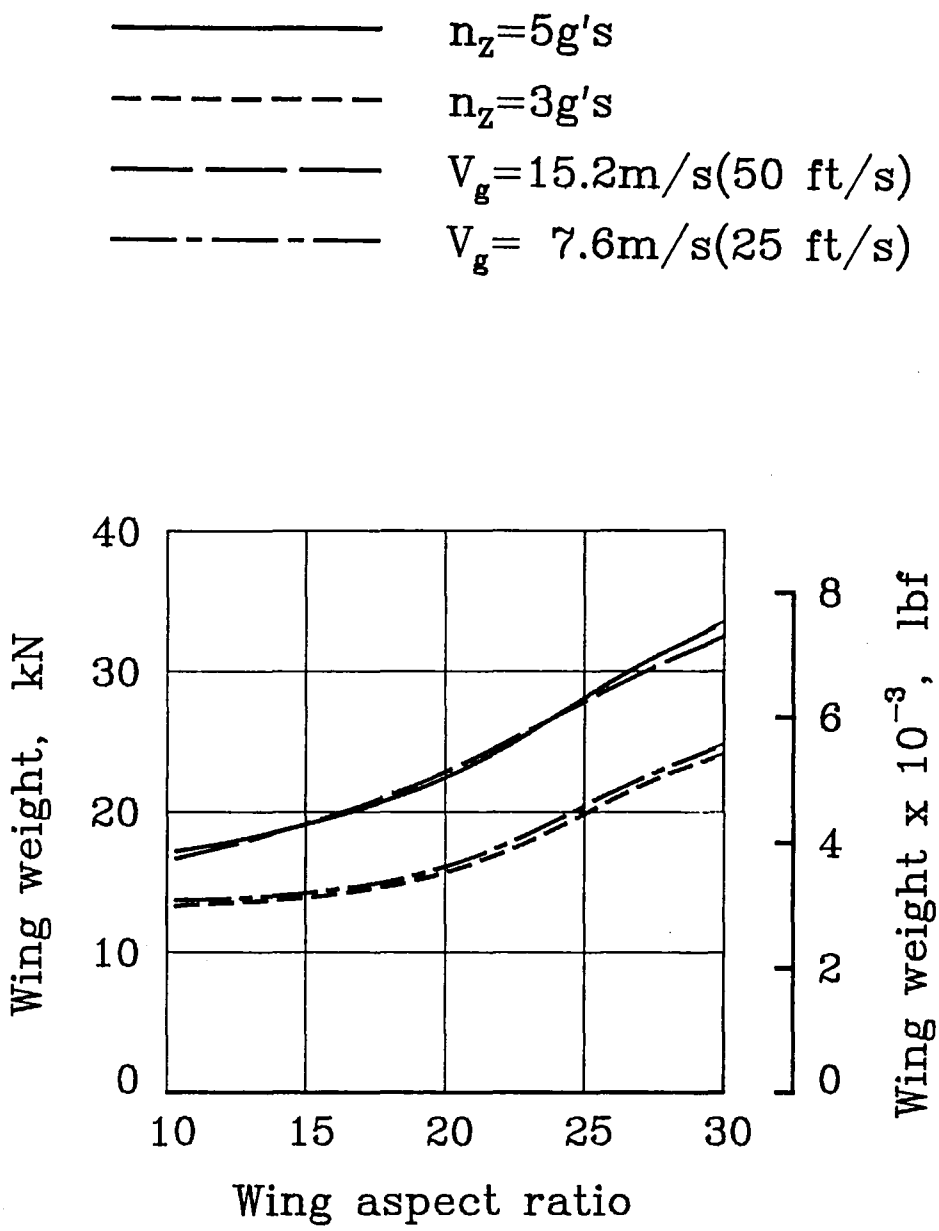

Figure 17. - Estimated cantilever wing weight as a function of design ultimate load factor; 94 percent full fuel condition , S = 57.6 m^2 (620 ft^2).

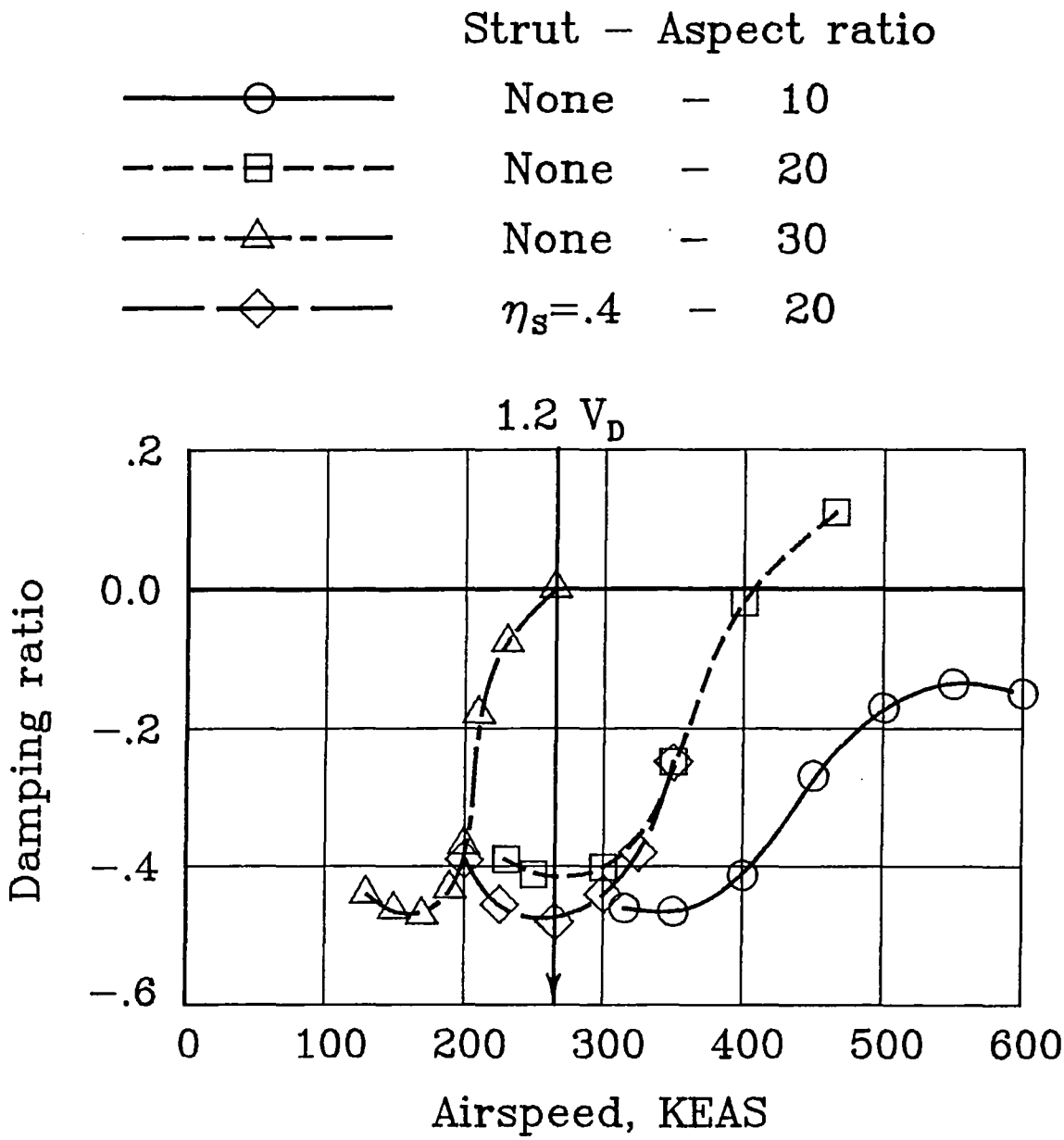

Figure 18. - Estimated effect of wing aspect ratio on configuration flutter characteristics; 94 percent full fuel condition, S = 57.6 m^2 (620 ft^2).

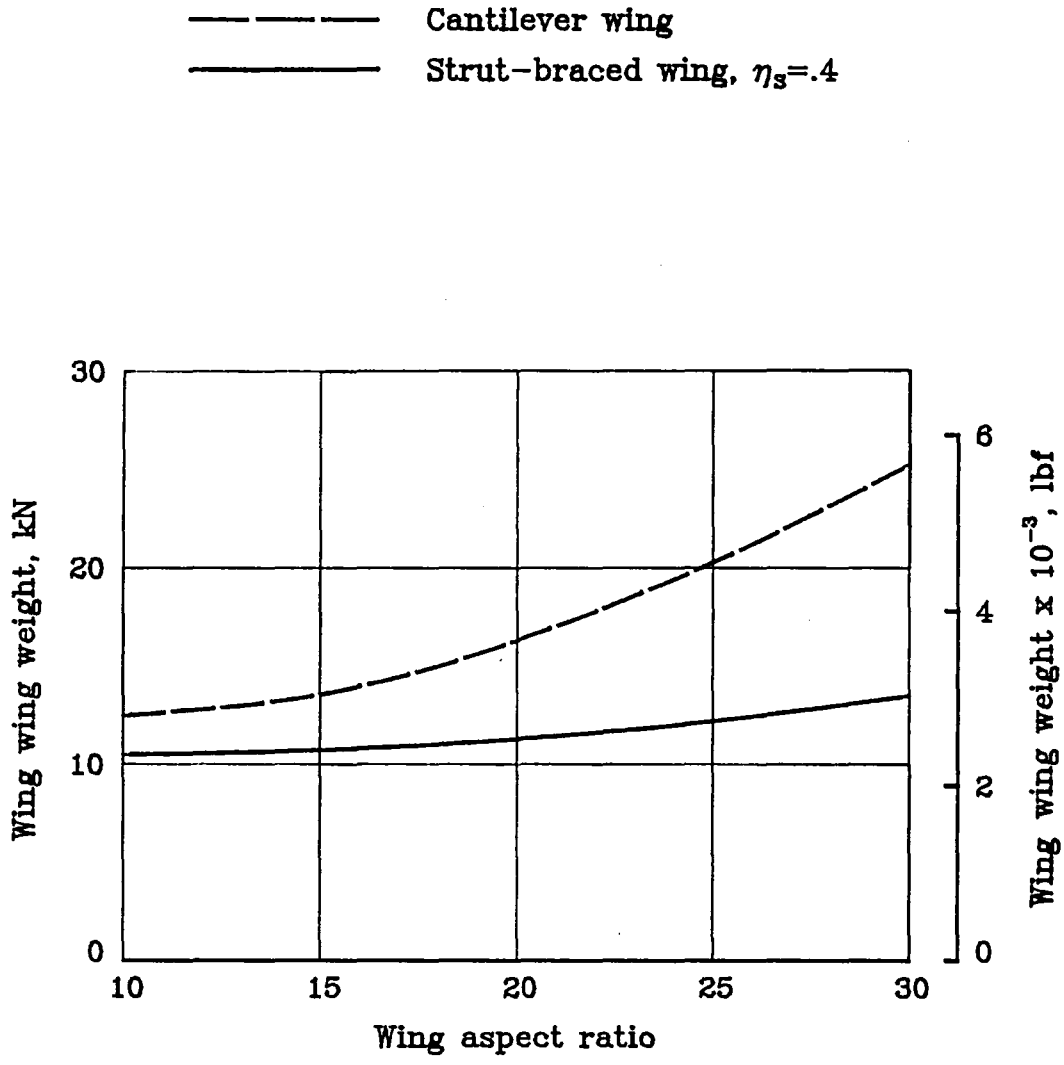

Figure 19. - Final estimated wing weights , S = 57.6 m^2 (620 ft^2).

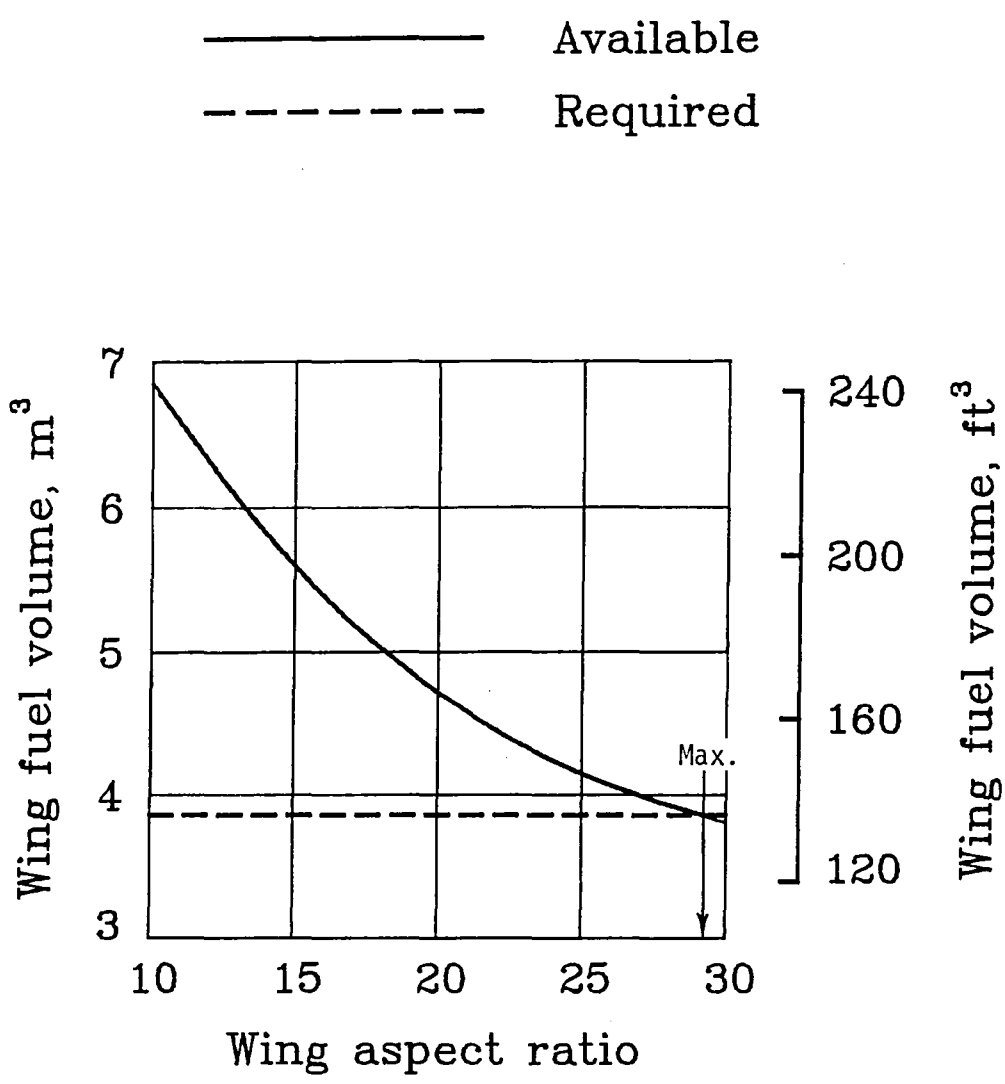

Figure 20. - Estimated wing fuel volume; t/c = 0.09, S = 57.6 m^2 (620 ft^2).

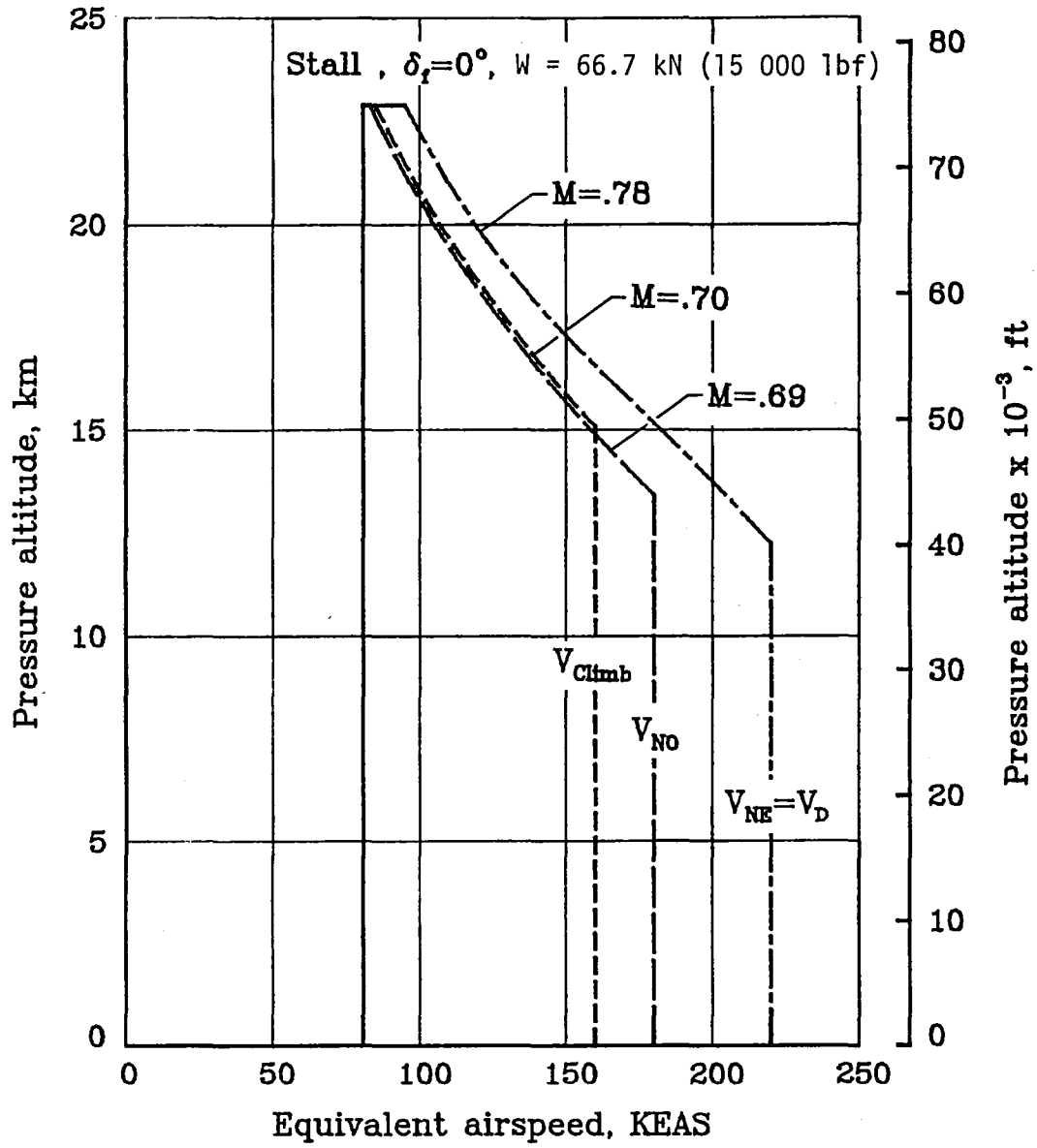

Figure 21. - Assumed baseline configuration flight envelope.

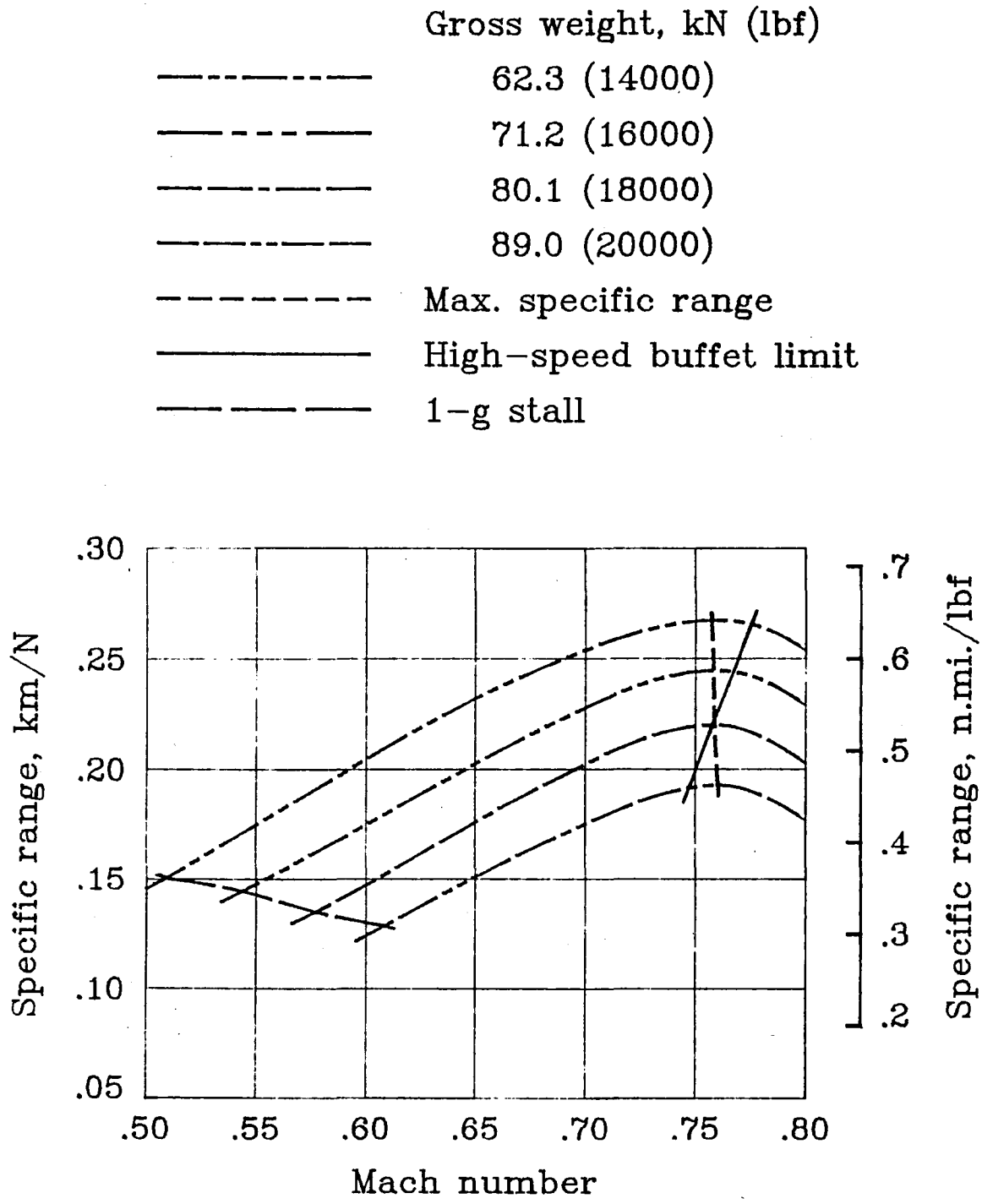

Figure 22. - Cruise specific-range capability of the baseline airplane at 19.8 km (65000 ft), S = 57.6 m^2 (620 ft^2).

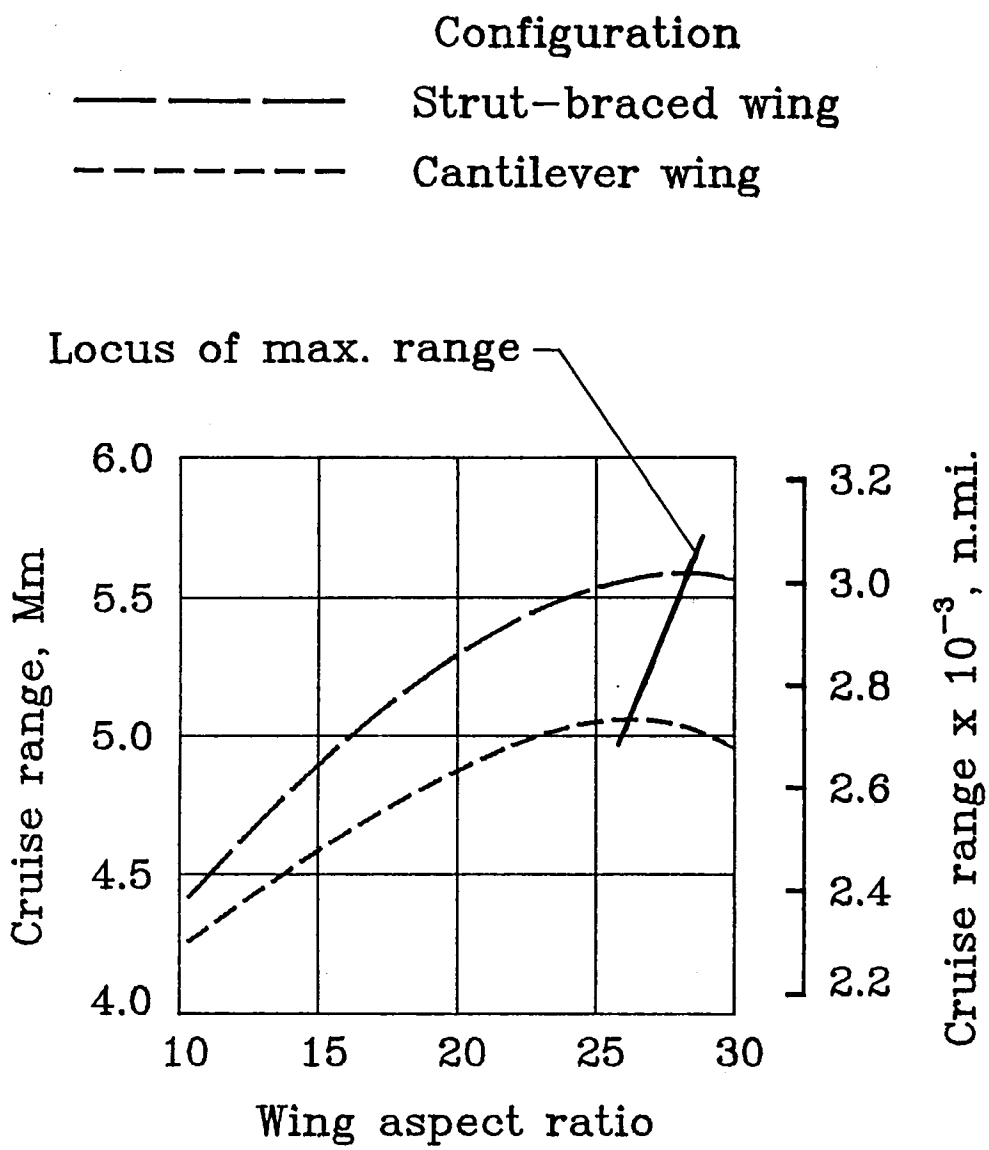

Figure 23. - Cruise range capability at M = 0.69 and 19.8 km (65 000 ft) altitude, S = 57.6 m^2 (620 ft^2).

APPENDIX A

LOW-SPEED WING DRAG DETERMINATION ASSUMING LAMINAR FLOW ON NACA 6-SERIES LOW-DRAG AIRFOILS

Paul M. Smith
Kentron International, Inc.
Hampton Technical Center

SUMMARY

A procedure is presented for estimating drag characteristics of cantilever-wings designed with NACA 6-series low-drag airfoils which have extensive natural laminar flow. The profile drag results are based on analysis of wind-tunnel test-determined airfoil characteristics.

ANALYSES

For many preliminary design purposes, it is permissible to represent the airplane drag polar as a simple parabolic curve defined by the equation

$$C_D = C_{D_{(C_L=0)}} + C_L^2/\pi Ae$$

The airplane efficiency factor, e, was introduced by W. Bailey Oswald (ref. A-1). This factor is used to account for wing potential-flow efficiency, airplane-component interference drag, and the growth of parasite drag with lift coefficient. The development, by the NACA, of the 6-series low-drag airfoils (ref. A-2) has resulted in the attainment of constant minimum drag levels over a lift-coefficient range displaced about the section design lift coefficient. This fact renders a simple parabolic drag approximation inappropriate, as shown in figure 18 of reference A-2.

An alternate approach to the estimation of low-speed wing drag coefficients uses three parameters. The first is a minimum obtainable profile drag, $C_{D_{p,min}}$, as a function of Reynolds number; the second is parasite drag, $C_{D_{pa}}$, which varies as a function of lift coefficient; and the third is the conventional induced drag based on a potential-flow efficiency factor, e_p, which is dependent on wing planform geometry. The resulting equation for wing drag coefficient is given as follows:

$$C_{D_{wing}} = C_{D_{p,min}} + C_{D_{pa}} + C_L^2/\pi A e_p$$

Minimum wing profile drag. - To determine the extent of smooth airfoil laminarization, two-dimensional drag test data were related to the predicted levels based on fully laminar and fully turbulent flows. The predicted drag levels were based on the following relationship,

$C_d = C_f\ f\ c_p/c$, where

f is the wing-profile form correction factor, herein as $1 + 1.5(t/c) + 125(t/c)^4$; t/c is the airfoil thickness-chord ratio; c_p/c is the ratio of the peripheral distance around the chord to the chord length, herein defined as $0.40(t/c) + 2.0$; and C_f is the flat-plate skin-friction-drag coefficient.

The flat-plate skin-friction-drag coefficients were estimated assuming that:

$$C_{f_{laminar}} = \frac{1.328}{[R]^{.5}}, \text{ and}$$

$$C_{f_{turbulent}} = \frac{0.455}{[\log_{10} R]^{2.58}}, \text{ where}$$

R is the Reynolds number based on the airfoil chord length.

The resulting extent of achievable laminar flow on airfoils is given in figure A-1. The data on smooth-airfoil laminarization, in percent, is presented as a function of Reynolds number for several specified NACA 6-series airfoils with various design lift coefficients and airfoil thickness-chord ratios. (Only the NACA 65-series derived test points are indicated; the additional lines represent fairings through their appropriate, unplotted, test points.) Other foil and flat-plate data were used to extend the curve to indicate transition to zero and 100 percent laminar flow levels. Note, the assumed fairing through the symbols indicates no effect of section thickness-chord ratio or airfoil design lift coefficient.

Using these derived results, the prediction of the wing minimum profile drag, $C_{D_{p,min}}$, is given as follows:

$$C_{D_{p,min}} = S_w f/S \left[C_{f_{turb}} - (C_{f_{turb}} - C_{f_{lam}})\bar{x}_{lam}/100 \right] , \text{ where}$$

$\bar{x}_{lam}$ is the percentage of achieved laminarization from figure A-1; S_w is the exposed wing wetted area; and S is the total wing area.

Parasite drag as a function of lift coefficient. - The growth of wing parasite drag with lift coefficient was determined by analyzing two-dimensional wind-tunnel test data on NACA 6-series airfoils. The incremental differences between section drag coefficient and drag coefficient at the design lift coefficient were determined for each airfoil as a function of lift coefficient for variations in section thickness-chord ratio, design lift coefficient, and Reynolds number. The resulting faired parasite drag increments for three NACA 6-series airfoils are plotted in figure A-2 as a function of lift coefficient increment from the airfoil design lift coefficient. Note, the minimum drag bucket is not symmetrical about the design lift coefficient. To account for changes in Reynolds number, this curve should be modified by adjusting the semi-width of the minimum drag bucket as indicated by the assumed line in figure A-3. The dashed line portion was drawn parallel to the solid line which represents test determined low-drag bucket semi-widths.

Induced drag. - The wing induced drag is herein defined as follows:

$C_{D_i} = C_L^2/\pi A e_p$, where

A is the wing aspect ratio, and e_p is the cantilever wing potential-flow efficiency factor.

In reference A-3, DeYoung presents aerodynamic charts for the accurate prediction of wing lift-curve slope, spanwise center of pressure location, and potential-flow wing efficiency factor for a wide range of wing planforms. The resulting potential-flow wing efficiency factors are presented in figure A-4 as a function of wing planform shape and aspect ratio.

REFERENCES

A-1. Oswald, W. Bailey: General Formulas and Charts for the Calculation of Airplane Performance. NACA Report No. 408, 1932.

A-2. Abbott, Ira H., von Doenhoff, Albert E., and Stivers, Louis, S., Jr.: Summary of Airfoil Data. NACA Report No. 824, 1945.

A-3. DeYoung, John: Wing Loading Theory Satisfying All Boundary Points. Ph.D. Dissertation, Department of Aerospace Engineering, The University of Texas at Arlington, 1975.

A-4. Van Dyke, Milton D.: High-Speed Subsonic Characteristics of 16 NACA 6-Series Airfoil Sections. NACA TN No. 2670, 1952.

A-5. Hoerner, Sighard F.: Fluid Dynamic Drag. Published by the author, Chapter 2, 1958.

A-6. Liebeck, Robert H.: Design of Subsonic Airfoils for High Lift. AIAA Journal of Aircraft, Vol. 15, September 1978, pp. 546-561.

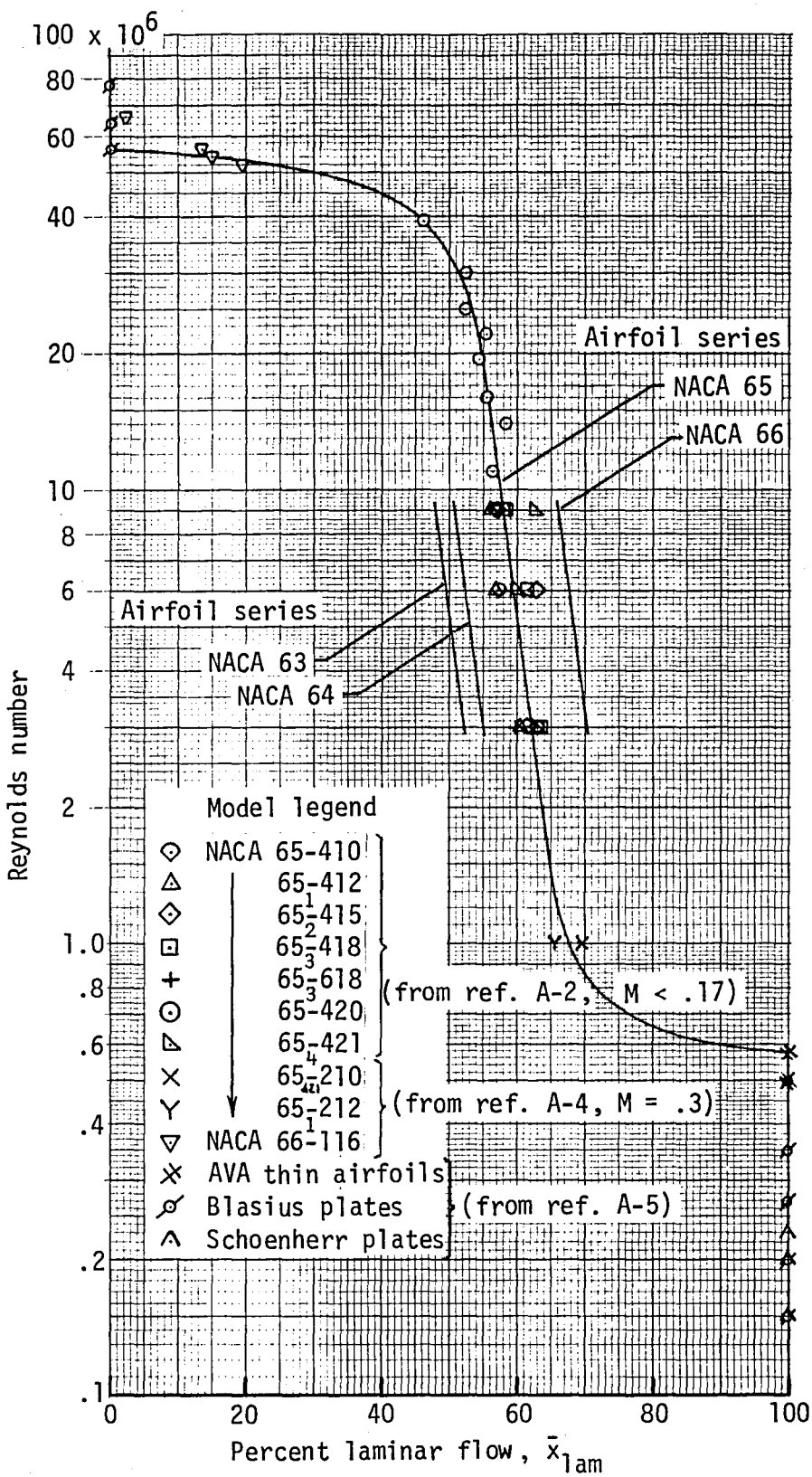

Figure A-1. - Derived extent of achieved laminar flow as a function of Reynolds number from incompressible-flow tunnel test results using smooth 2-dimensional models.

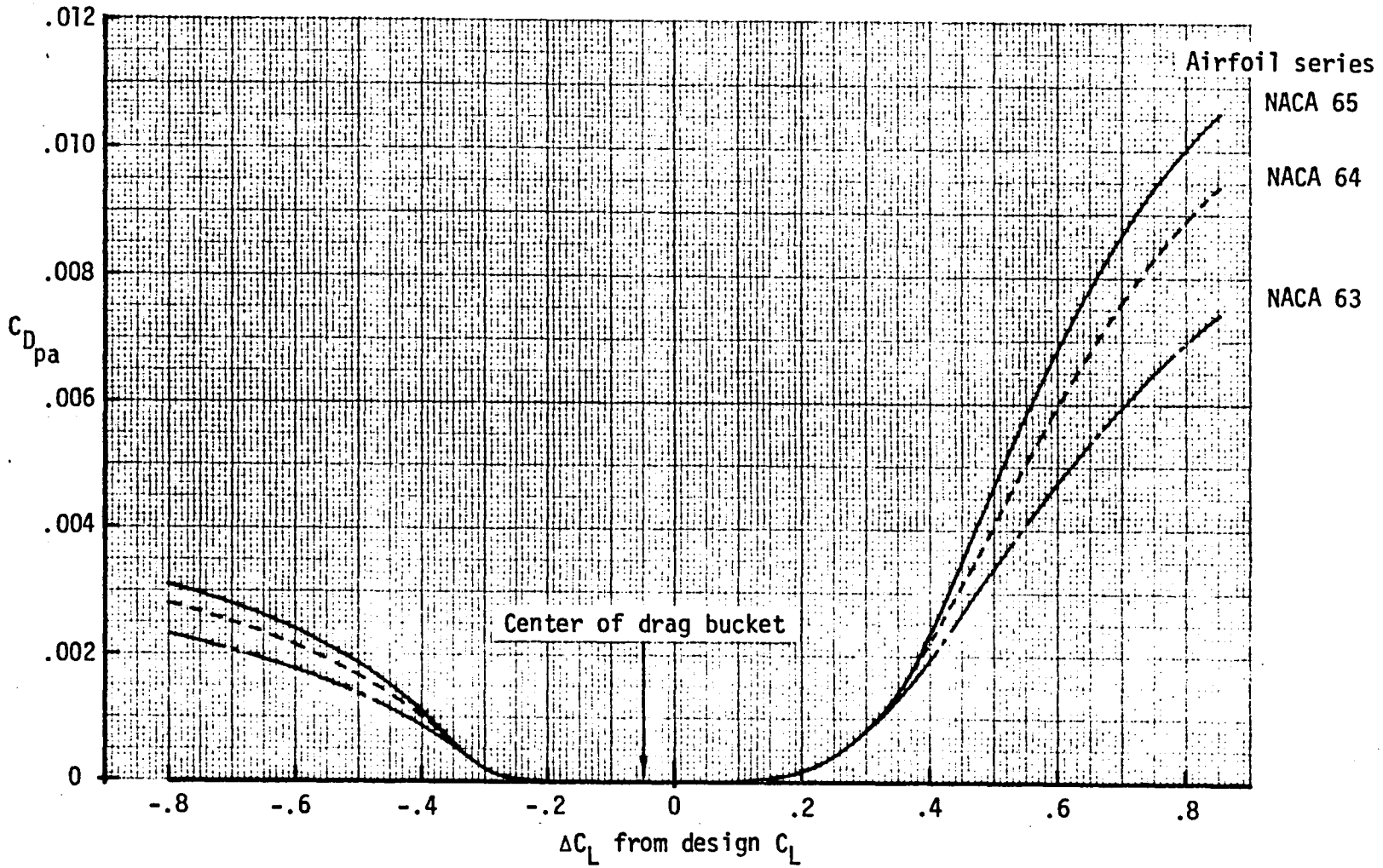

Figure A-2. - NACA 6-series airfoil parasite drag characteristics, RN = 6 x 10^6; lines represent fairings through test data from reference A-2.

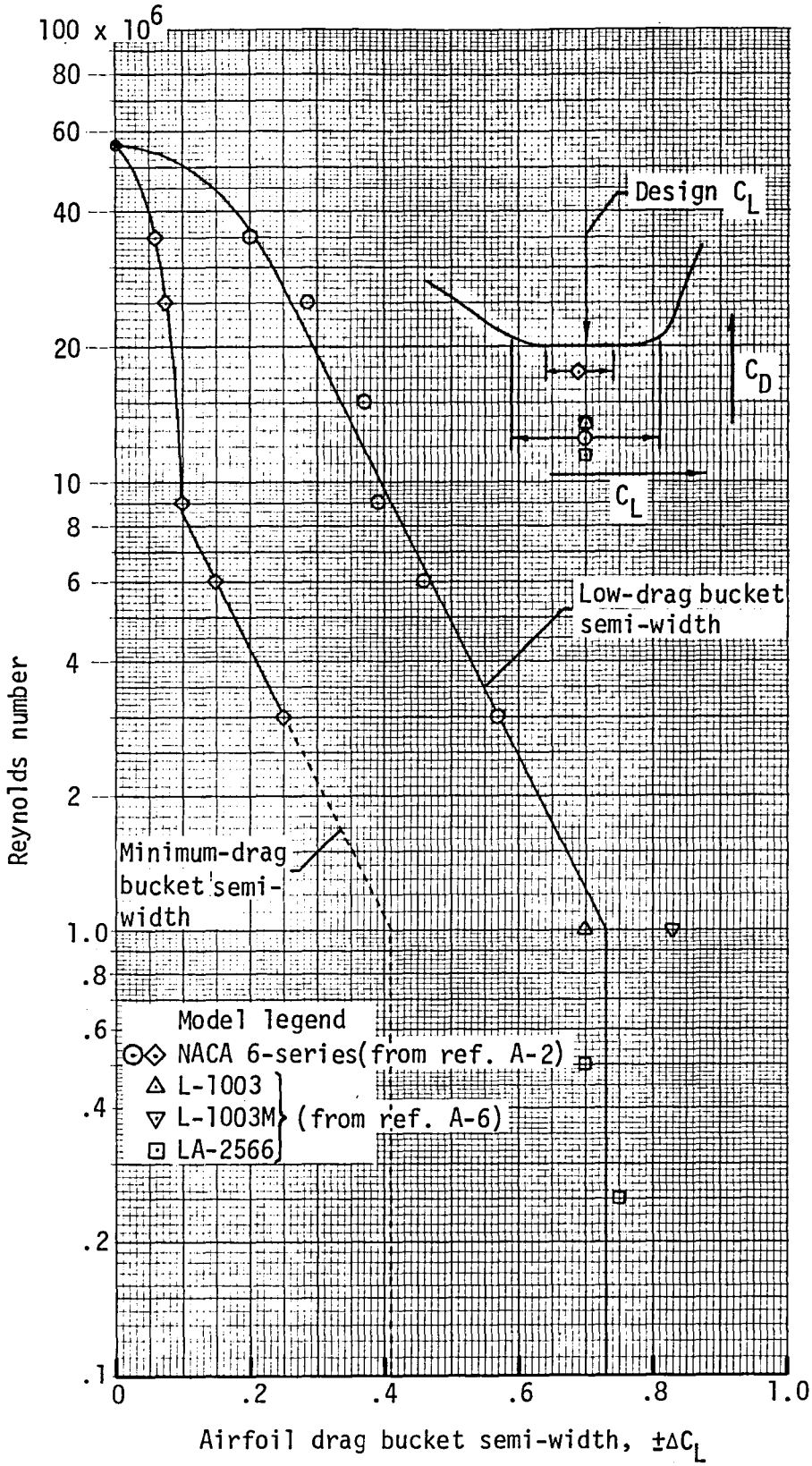

Figure A-3. - Derived variation of airfoil drag bucket semi-width as a function of Reynolds number.

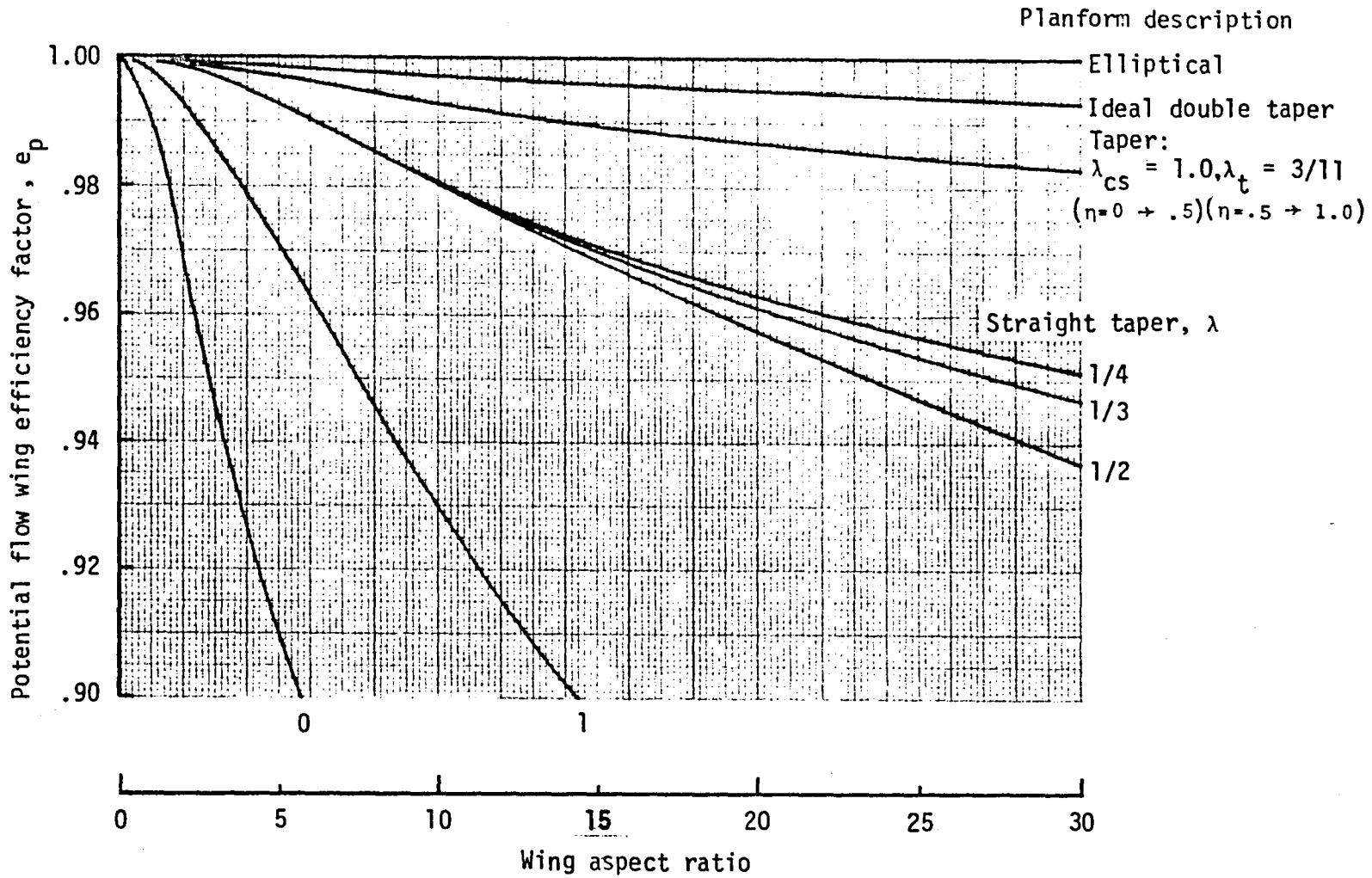

Figure A-4. - Potential-flow wing efficiency factor as a function of wing planform shape and aspect ratio.

APPENDIX B

AERODYNAMICS OF A WING WITH LIFTING STRUTS

John DeYoung
Kentron International, Inc.
Hampton Technical Center

SUMMARY

An approximate analysis is developed for estimating lift-to-drag ratios of wings with struts. At aircraft design lift coefficient, the spanwise loading along the strut span is made uniform by a moderate strut twist. The ratios of lift to drag of aircraft with and without wing struts provides a measure of strut effectiveness. This lift-to-drag ratio depends on strut lift, wing lift, and profile drags of strut, wing, and fuselage plus appendages. The results show that a gain in lift-to-drag ratio can be realized by having lift on the strut as compared to no lift on the strut. This gain is of the same nature as that of a biplane with the lower wing lifting as compared to not lifting.

SYMBOLS

A	wing aspect ratio
a	wing lift-curve-slope, $dC_L/d\alpha$
b	wing span, m
C_D	drag coefficient, $D/(\frac{1}{2}\rho V^2 S)$
C_L	lift coefficient, $L/(\frac{1}{2}\rho V^2 S)$
D	drag, N
e	wing efficiency factor
G	dimensionless spanwise loading distribution
H	dimensionless strut vertical dimension, h/b
h	strut vertical dimension, m

L	lift, N
M	Mach number
S	wing area, m^2
V	freestream velocity, m/sec
v	sidewash in far field (Trefftz plane), m/sec
w	downwash in far field (Trefftz plane), m/sec
y	spanwise wing dimension, m
z	vertical wing dimension, m
α	wing angle of attack, deg
γ	angle between strut and wing, deg
ε	strut section angle relative to wing reference angle, deg
ζ	dimensionless strut vertical station, z/(b/2)
η	dimensionless strut spanwise station, y/(b/2)
Λ	wing sweep angle of 50% chordline, positive rearward, deg
ρ	mass density of air, kg/m^3

Subscripts

a	value for aircraft without wing
av	average
bi	biplane
d	design
i	induced
mon	monoplane
max.	maximum
o	parasite component
s	strut or strut attachment point
so	strut value at design point

tw	twist
w	wing
ws	wing influence on strut or wing plus strut

ANALYSES

The yz-plane view of the wing with strut support of the wing is shown in figure B-1. The strut aerodynamic loading along the strut is defined to be uniform on the exposed struts and to blend into the wing loading from y_s to the wingtip. Thus there is no trailing vorticity sheet from the exposed strut.

Lift and Drag of Wing with Struts

The wing-strut combination acts as a kinked-wing biplane, as shown here.

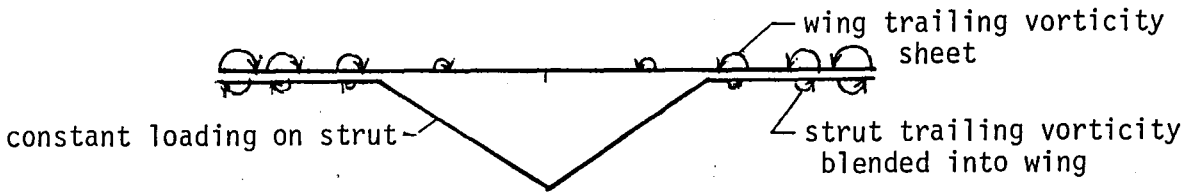

With these assumptions, there is no strut-induced velocity at the wing trailing sheet; however, there is a wing trailing-sheet induced velocity at the strut position. This constraint is applied to simplify the analytic development that follows.

Induced angle of attack. - Far downstream of the wing, the induced angle at the strut due to the wing is expressed as

$$\alpha_{i,ws} = \frac{w}{V}\cos\gamma + \frac{v}{V}\sin\gamma \qquad \text{(B1)}$$

For small vertical distances from the downwash sheet, approximations may be developed for the downwash and sidewash angle (as given on page 53 of ref. B-1). These may be coupled with the assumption of wing elliptic loading (i.e., $G = (2C_{L_w}/\pi A)\sqrt{1-\eta^2}$) and equation (B1) rewritten as

$$\alpha_{i,ws} = \frac{2C_{L_w}}{\pi A}\left\{\left[1 - \frac{|\zeta|}{(\sqrt{1-\eta^2})^3}\right]\cos\gamma + \frac{|\eta|}{\sqrt{1-\eta^2}}\sin\gamma\right\} \tag{B2}$$

As can be seen from figure B-1, the strut displacement function is

$$\zeta = (|\eta| - \eta_s)\tan\gamma \tag{B3}$$

Equation (B2) then becomes

$$\alpha_{i,ws} = \frac{2C_{L_w}\cos\gamma}{\pi A}\left[1 - \frac{(\eta_s - |\eta|)\tan\gamma}{(\sqrt{1-\eta^2})^3} + \frac{|\eta|\tan\gamma}{\sqrt{1-\eta^2}}\right] \tag{B4}$$

The average induced angle aft of the wing at the strut location is

$$\alpha_{i,ws,av} = \frac{1}{\eta_s}\int_0^{\eta_s}\alpha_{i,ws}\,d\eta = \frac{2C_{L_w}}{\pi A}\cos\gamma \tag{B5}$$

These induced angles are between freestream direction and the strut chord.

Strut twist and lift. - The required strut twist which results in uniform strut spanwise loading on the exposed strut is written as

$$\varepsilon_{s,tw} = \frac{1}{2}(\alpha_{i,ws} - \alpha_{i,ws,av}) = \frac{C_{L_w}\sin\gamma}{\pi A}\left[-\frac{\eta_s - |\eta|}{(\sqrt{1-\eta^2})^3} + \frac{|\eta|}{\sqrt{1-\eta^2}}\right] \tag{B6}$$

Since this strut has no trailing-vorticity sheet, there is no induced angle due to the strut. However, induced velocity due to the wing trailing-vortex sheet acts on the strut. The lift coefficient of the strut is

$$C_{L_s} = 2\pi\left(\alpha_s - \frac{1}{2}\alpha_{i,ws,av}\right) \tag{B7}$$

where α_s is the strut angle of attack of strut chord relative to free stream direction, and the induced angle is given in equation (B5). The solution for the averaged strut angle, α_s, from equations (B7) and (B5) is

$$\alpha_s = \frac{C_{L_w}}{2\pi}\left(\frac{C_{L_s}}{C_{L_w}} + \frac{2}{A}\cos\gamma\right) \tag{B8}$$

The $\alpha_s(\eta)$ distribution along the span of the strut may be given by the sum of mean and local increments. At design C_L, this is written as

$$\alpha_s(\eta) = \frac{C_{L_{wd}}}{2\pi}\left\{\frac{C_{L_{sd}}}{C_{L_{wd}}} + \frac{2}{A}\cos\gamma - \frac{2}{A}\sin\gamma\left[\frac{\eta_s - |\eta|}{(1-\eta^2)^{3/2}} - \frac{|\eta|}{(1-\eta^2)^{1/2}}\right]\right\}\frac{a_w(M=0)}{a_w(M)} \tag{B9}$$

which includes a factor for approximating the effect of Mach number. This gives the strut angle of attack along the strut span such that uniform strut spanwise loading is realized.

The strut lift as a function of α is obtained from equation (B7). Then with $\alpha_s = \alpha\cos\gamma + \alpha_{so}$, an approximation for C_{L_s} when α is not at design value, α_d, is

$$C_{L_s} = 2\pi\left[\left(1 - \frac{a_w}{\pi A}\right)\frac{C_{L_w}}{a_w}\cos\gamma + \alpha_{so}\right] \tag{B10}$$

where α_{so} is determined at the design C_L. Thus with equation (B8)

$$\alpha_{so} = \alpha_{s,d} - \alpha_d\cos\gamma = \alpha_{s,d} - \frac{C_{L_{w,d}}}{a_w}\cos\gamma$$

$$= \frac{C_{L_{w,d}}}{2}\left(\frac{C_{L_{s,d}}}{C_{L_{w,d}}} + \frac{2}{A}\cos\gamma - \frac{2\pi}{a_w}\cos\gamma\right) \tag{B11}$$

Thus an off-design value of strut lift coefficient for off-design wing lift coefficients can be estimated from equation (B10) in which α_{so} is determined from equation (B11) in terms of design wing and strut lift coefficients.

Total lift. - The aircraft total lift coefficient for small γ is given by

$$C_L = C_{L_w} + \frac{S_s}{S_w} C_{L_s} \tag{B12}$$

where C_L and C_{L_w} are based on wing area and C_{L_s} on strut area. This result may be used in equation (B10) to obtain the wing lift coefficient in terms of total lift coefficient. Then

$$C_{L_w} = \frac{C_L - 2\pi \frac{S_s}{S_w} \alpha_{s_0}}{1 + 2\pi \frac{S_s}{S_w} \left(\frac{1}{a_w} - \frac{1}{\pi A}\right)} \tag{B13}$$

where α_{s_0} is obtained from equation (B11). As an example, for a minus one-g lift, $C_L qS_w = -W$, and C_{L_w} is determined from equation (B13), then C_{L_s} from eqation (B10). The strut contribution to aircraft lift is $L_s = qS_s C_{L_s}$, and at small γ the force normal to this strut is $qS_s C_{L_s}$. From reference B-2, an accurate equation for wing lift-curve-slope for elliptic wings is

$$\left.\begin{aligned} a_w = \frac{dC_{L_w}}{d\alpha} = \frac{2\pi A}{A' + 2k}, \qquad k = \frac{A + 3.78}{A + 1.89} \\ \text{where the effects of compressibility and sweep are approximated by} \\ A' = \frac{A}{\cos \Lambda_{1/2}} \sqrt{1 - M^2 \cos^2 \Lambda_{1/2}} \end{aligned}\right\} \tag{B14}$$

Total lift and drag. - It is assumed that the strut influence on the wing is small, such that the wing of this wing-strut configuration maintains elliptic spanwise loading. Then the wing induced drag is

$$C_{D_{i,w}} = \frac{C_{L_w}^2}{\pi A} \tag{B15}$$

To this is added the induced drag due to wing induced angle on the strut. Because it is assumed that the lateral loading distribution on the strut is uniform, then the induced angle and induced drags due to the strut on the wing and the strut on the strut are negligible. Hence the total induced drag coefficient is

$$C_{D_i} = \frac{C_{L_w}^2}{\pi A} + \frac{S_s}{S_w} C_{L_s} \frac{\alpha_{i,ws,av}}{2} \tag{B16}$$

The total lift coefficient for small γ is

$$C_L = C_{L_w} \left(1 + \frac{S_s}{S_w} \frac{C_{L_s}}{C_{L_w}}\right) \tag{B17}$$

Using equations (B5) and (B17), equation (B16) becomes

$$C_{D_i} = \frac{C_{L_w}^2}{\pi A} + \frac{S_s}{S_w} \frac{C_{L_s} C_{L_w}}{\pi A} = \frac{C_L^2}{\pi A \left(1 + \frac{S_s}{S_w} \frac{C_{L_s}}{C_{L_w}}\right)}$$

thus the approximation for total induced drag coefficient for small $S_s C_{L_s} / S_w C_{L_w}$ ratios is

$$C_{D_i} = \frac{C_L^2}{\pi A e} \tag{B18}$$

where

$$e = 1 + \frac{S_s}{S_w} \frac{C_{L_s}}{C_{L_w}} \tag{B19}$$

The wing alone total drag coefficient is

$$C_{D_w} = C_{D_{o,a}} + C_{D_{o,w}} + \frac{C_{L_w}^2}{\pi A} \tag{B20}$$

The total drag coefficient for the wing with struts is

$$C_D = C_{D_{o,a}} + C_{D_{o,w}} + \frac{S_s}{S_w} C_{D_{o,s}} + \frac{C_L^2}{\pi A e} \qquad \text{(B21)}$$

(Note that subscript w refers to the wing, and subscript s to the strut.)

The ratio $S_s C_{L_s} / S_w C_{L_w}$ represents the lift ratio L_s/L_w. There is a value for the lift ratio at which e is maximum. Because of the approximations used in the simplified derivation of equation (B19) for small lift ratios, such a maximum is undefined (reference B-3 has exact detailed theory). An estimate of effective lift ratios at which e is maximum can be approximated from available biplane data of wings of unequal spans. A statistical analysis of the biplane data results in the approximate functions given by

$$\frac{L_s}{L_w} = \left|\eta_{s,av}\right|^{\left(2 + \frac{\eta_s + 4\eta_{s,av}}{8.5H^{.8}}\right)} \qquad \text{(B22)}$$

$$\left(\frac{S_s C_{L_s}}{S_w C_{L_w}}\right)_{\substack{\text{effective} \\ \text{for } e_{max}}} = 2.6\, H_{av}^{\eta_s} \left|\eta_{s,av}\right|^{\left(2 + \frac{\eta_s + 4\eta_{s,av}}{8.5H^{.8}}\right)} \qquad \text{(B23)}$$

where $H_{av} = h_{av}/b$, and $\eta_{s,av}$ is the dimensionless averaged span extent of the strut. An estimate of maximum e is obtained with equation (B19) using equation (B23). The maximum e occurs at the approximate strut-lift to wing-lift ratio given in equation (B22). In equation (B19) using values of $S_s C_{L_s} / S_w C_{L_w}$ larger than those given in equation (B23) result in estimates for e which are optimistic.

Maximum L/D ratios. - For the wing alone, based on equation (B20), the wing lift coefficient for maximum L/D is

$$C_{L_{\text{max L/D, w}}} = \left[\pi A (C_{D_{o,a}} + C_{D_{o,w}})\right]^{1/2} \qquad \text{(B24)}$$

therefore,

$$\left(\frac{L}{D}\right)_{max,w} = \frac{1}{2}\left(\frac{\pi A}{C_{D_{o,a}} + C_{D_{o,w}}}\right)^{1/2} \tag{B25}$$

For the wing plus struts, based on equation (B21)

$$C_{L_{max\ L/D,\ ws}} = \left[\pi Ae\left(C_{D_{o,a}} + C_{D_{o,w}} + \frac{S_s}{S_w} C_{D_{o,s}}\right)\right]^{1/2} \tag{B26}$$

therefore

$$\left(\frac{L}{D}\right)_{max,ws} = \frac{1}{2}\left(\frac{\pi Ae}{C_{D_{o,a}} + C_{D_{o,w}} + \frac{S_s}{S_w} C_{D_{o,s}}}\right)^{1/2} \tag{B27}$$

where e is given in equation (B19). The ratios of equations (B26) to (B24) and (B27) to (B25) are

$$\frac{C_{L_{max\ L/D,ws}}}{C_{L_{max\ L/D,w}}} = e^{1/2}\left(1 + \frac{\frac{S_s}{S_w} C_{D_{o,s}}}{C_{D_{o,a}} + C_{D_{o,w}}}\right)^{1/2} \tag{B28}$$

$$\frac{(L/D)_{max,ws}}{(L/D)_{max,w}} = e^{1/2}\left(1 + \frac{\frac{S_s}{S_w} C_{D_{o,s}}}{C_{D_{o,a}} + C_{D_{o,w}}}\right)^{-1/2} \tag{B29}$$

In equation (B29) the maximum lift to drag ratio of the airplane with wing plus struts is compared to that with wing alone. Relatively,it is seen that the maximum lift-to-drag ratio of the wing with struts increases with some lift on the struts (since then e increases,see equation B19) and also increases as the added airplane drag coefficient, $C_{D_{o,a}}$ (drag of airplane without wing) increases.

REFERENCES

B-1. DeYoung, John, and Barling, W. H. Jr.: Prediction of Downwash Behind Swept-Wing Airplanes at Subsonic Speeds. NACA TN-3346, 1955.

B-2. DeYoung, John: Wing Loading Theory Satisfying all Boundary Points. Ph.D. Dissertation, Department of Aerospace Engineering, The University of Texas at Arlington, 1975.

B-3. DeYoung, John: Minimization Theory of Induced Drag Subject to Constraint Conditions. NASA CR-3140, 1979.

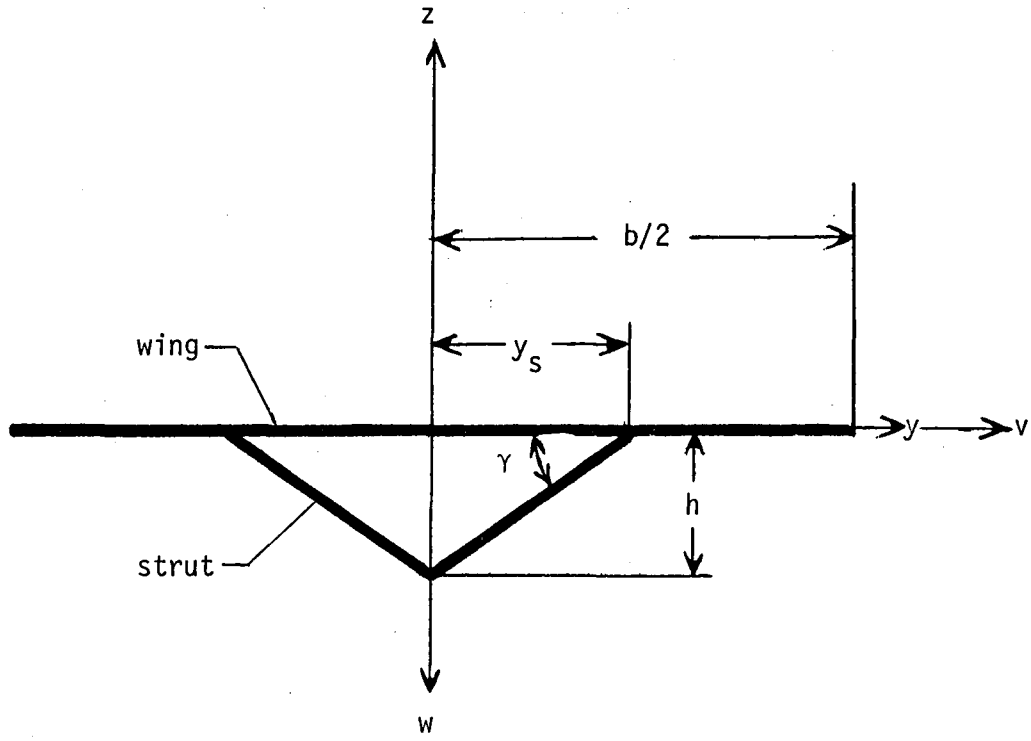

Figure B-1.- Dimensional geometry of the wing plus struts, view from aft of wing.

APPENDIX C

WEIGHT PREDICTION METHODOLOGY OF WINGS AND WING STRUTS WITH EXAMPLE DETAILED WEIGHTS

Jack E. Price and G. Fred Washburn
Kentron International, Inc.
Hampton Technical Center

A procedure for estimating the weight of cantilever and strut-braced wings and wing struts is presented. Certain detailed weights for specific configurations are also formulated.

Wing Weight

Initially, the wing structural weight for a conventional cantilever wing vehicle was determined utilizing an unpublished mass properties computer program. The method was based on a statistically derived wing weight equation of the form:

$$\text{Wing weight} = f\left[\frac{W^a S^b A^c (n_{z_{ult}})^d}{(t/c)^e \cos\Lambda}\right], \text{ where:}$$

W = design gross weight

S = wing area

A = wing aspect ratio

$n_{z_{ult}}$ = ultimate load factor

t/c = airfoil streamwise thickness-chord ratio

Λ = sweep angle of the 25 percent chord

a,b,c,d,e = constant exponents

From the above equation an initial wing weight was derived and a structural relief load was determined. The structural relief load was used in the wing bending moment equation of the form:

Wing bending moment, $W_{bm} = f(Wy_1 - Iy_2)$, where:

I = total wing relief load (structure plus fuel)

y_1 = centroid of the airload

y_2 = centroid of the wing weight

A final cantilever wing weight was then determined by the following equation:

Wing weight = $f\left[W_{bm}^{g} A^{h} M^{i} (t/c)^{j}\right]$, where:

M = Mach number

g,h,i,j = constant exponents

These three equations were then cycled, as required, to refine wing weight accuracy.

Previous experience with the above equations, and the basic computer program, have shown good correlation with existing wing weights for low, less than 10, aspect ratio wings. For the high aspect ratio wings of interest in this study, the equations, noted above, under-predict the wing structural weight and therefore required modification. The approach taken for modification was:

1. Strength size conventional cantilever wings with aspect ratios of 10, 20, 25, and 30 using established loads, such as table C-I and the SPAR structural Analysis System (ref. C-1).

2. From SPAR determine the slope of the structural weight versus aspect ratio curve.

3. Utilize this slope information to modify the weight equations in the mass properties computer program.

This approach was validated by simulating the T-39D twin engine turbojet trainer. This aircraft was chosen because actual detailed wing weight data was available, reference C-2. This simulation provided an adequate means for establishing the strength allowables used in determining the wing skin thickness and weight. Equation 7.17 of reference C-3 was utilized in determining the wing skin thickness:

$$\bar{t} = C_c L_o + \left(\frac{N_c}{F_{co}} \right) UF, \text{ where:}$$

$\bar{t}$ = wing skin thickness, cm (in.)

C_c = constant

L_o = rib spacing

N_c = running load, N/m (lbf/in.)

F_{co} = strength allowable, N/m^2 ($lbf/in.^2$)

UF = ultimate factor of 1.5

An ultimate strength allowable of 206.9 MP_a (30 000 psi) was selected for the wing structural material based on the results of the T-39D simulation. Representative values of ultimate stress allowable for most aircraft structural material ranges from 379.3 to 538 MPa (55 000 to 78 000 psi). Good correlation with estimations was achieved in accounting for non-optimum weight material in the T39D simulation. Non-optimum weight items consist of non-tapered skins, fasteners, joint pad-ups, tolerances, brackets, etc., and have proven to be a fairly large portion of the total wing structural weight.

Once the strength allowable had been established and the mass properties program modified, the high-aspect-ratio strut-braced wings were evaluated, and final vehicle weights were established. The method used for determining final wing and strut weights was as follows:

1. At each aspect ratio, using SPAR and the equation for determining the wing thickness, size the structure for both the cantilever and strut-braced wing.

2. Determine the difference in wing skin weight between the cantilever and strut-braced wing. (See table C-II for typical example.)

3. Determine the strut-braced wing weight. Strut-braced wing weight = [weight of cantilver wing (from mass properties program)] + [strut weight, table C-III] - [wing skin weight savings].

4. Determine gust, flutter, and deflection requirements and modify wing weight as required to satisfy these criteria.

Strut Weight

The structural sizing and, consequently, the weights of long, braced lifting struts subjected to column compression loads and concurrent transverse airloads were determined by beam-column theory. This method was selected as being a realistic approach to determine an objective weight assessment of a strut-braced wing strut. The design criteria were a lifting strut with design loads resulting from column compression and concurrent transverse airloads due to a -1g maneuver. The strut lengths were determined from the design layouts.

The following design decisions were established:

- Consider only thickness-chord ratios of 9 and 12 percent to minimize the increase in drag-rise-inception Mach number.
- Consider only a range of strut chords of .457 m (18 in.) to .737 m (29 in.) for compatability with the aerodynamics of a high-aspect-ratio wing braced with lifting struts.
- Fix the wing-strut attachment location at .4(b/2) for wings with A = 20, 25, and 30 resulting in strut lengths of 6.25 m (20.5 ft), 7.04 m (23.1 ft), and 7.72 m (25.3 ft), respectively.

To obtain the desired strut chords, thickness-chord ratios, and reasonable weights for the required strut lengths, one or more side stabilizing braces were necessary.

The -1g maneuver loading and the manner of support for a wing strut with a single mid-span side-stabilizing brace, or two equally spaced side-stabilizing braces, is shown below.

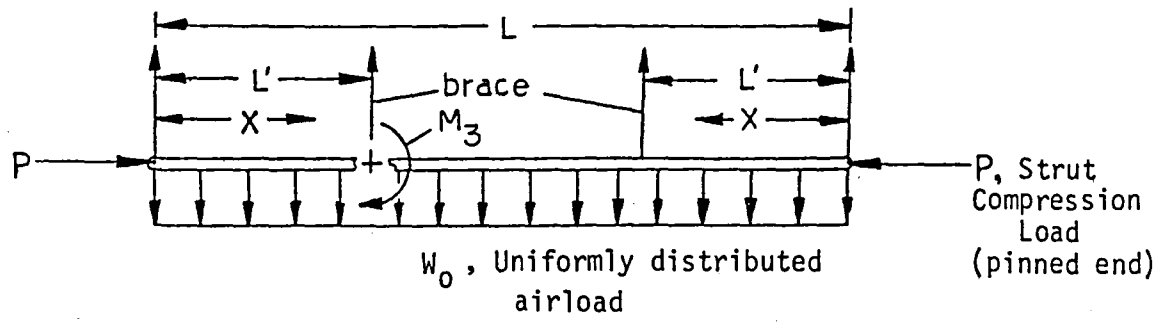

L' = L/3.28 for two side-stabilizing braces.

L' = L/2 for a single mid-span stabilizing brace.

Max. M = M_3 occurs at X = L'.

The equation for calculating M_3 is:

$$\text{Max.M} = M_3 = W_o L' j \left\{ \frac{\tan \frac{L'}{j} \left[\tan\left(\frac{L'}{2j}\right) - \frac{L'}{2j} \right]}{\tan\left(\frac{L'}{j}\right) - \frac{L'}{j}} \right\}$$, reference C-4, where:

$$j = \sqrt{\frac{EI}{P}}$$

The maximum compressive bending stress, $(f_c) = H_3 c/I + P/A$, occurred in the strut-box skins for the critical design condition of -1g maneuver. Figure C-1 shows the wing-strut structural box arrangement and the secondary leading- and trailing-edge structure. Table C-IV lists the wing strut dimensional and weight data. All the struts listed in table C-IV, without the side-stabilizing braces, would be unstable in column bending, even with solid aluminum structural boxes.

The strut side-stabilizing brace critical design load condition was determined to be the compression loads resulting from a +2g maneuver. The side braces were assumed to be pinned to the strut and to the wing, and positioned 90° to the strut.

The +2g maneuver loading, and the manner of support for a single strut with a single mid-span side stabilizing brace, or two equally spaced side stabilizing braces, is shown below.

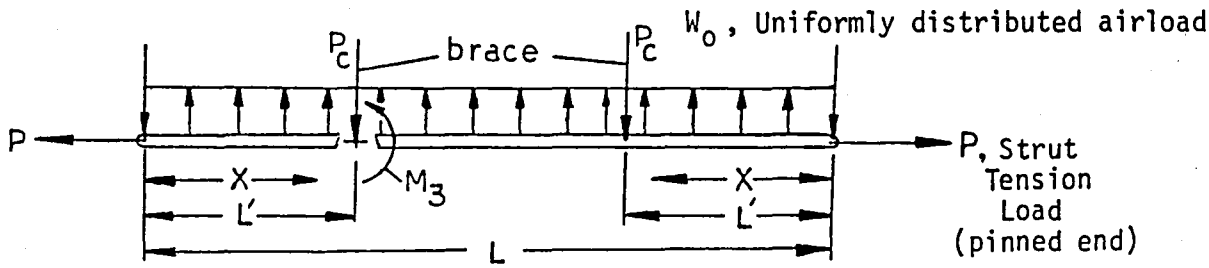

L' = L/3.28 for two side-stabilizing braces.

L' = L/2 for a single mid-span stabilizing brace.

Max.M = M_3 occurs at X = L'.

$P_c = W_o L'/2 + M_3/L'$.

The equation used for calculating M_3 is:

$$\text{Max.M} = M_3 = -W_o L' j \left\{ \frac{\tanh \frac{L'}{j} \left[\frac{L'}{2j} - \tanh \frac{L'}{2j} \right]}{\tanh\left(\frac{L'}{j}\right) - \frac{L'}{j}} \right\} \text{, where:}$$

$$j = \sqrt{\frac{EI}{ABS(P)}} \text{, for P negative}$$

Representative symmetrical airfoils with thickness-chord ratios of 9 and 12 percent of .05 m (2.0 in.), .08 m (3.0 in.), .10 m (4.0 in.), and .13 m (5.0 in.) were selected for structural sizing of the side-stabilizing braces. The braces

consisted of symmetrical airfoil shaped aluminum skins with no internal supporting structure, the skins remaining stable at the +2g maneuver limit compression loads. Lengths of the braces were determined by design layout.

The sectional area of the brace was obtained from Euler's theory of long columns in compression.

$$A = \frac{P_c L_1^2}{\pi^2 E \rho^2} = \frac{P_c L_1^2}{\text{constant} \times \rho^2}$$, reference C-5, where:

ρ = constant$_1$ x (brace chord)

constant$_1$ = f(t/c)

L_1 = length of brace (pin center to pin center)

The equation for calculating the brace skin thickness is:

$$t_{skin} = \frac{A}{\text{constant}_2 \times (\text{brace chord})}$$, where:

constant$_2$ = f(t/c)

Table C-V presents the dimensional and weight data of the strut braces sized by the above method for the wings with aspect ratios of 20, 25, and 30, respectively.

REFERENCES

C-1. Whetstone, W. D.: SPAR Structural Analysis System Reference Manual, System Level 14. NASA CR-145098, 1979.

C-2. North American Aviation, Inc.: Actual Weight and Balance Report for a Twin Engine Turbojet Radar Trainer, T-39D. North American Report NA-63-111, 1963.

C-3. Shanley, F. R.: Weight-Strength Analysis of Aircraft Structures. Dover Publications, Inc., 1960.

C-4. Roark, Raymond J.: Formulas for Stress and Strain. McGraw-Hill Book Company, Inc., 1954.

C-5. Bruhn, E. F., et.al.: Analysis and Design of Aircraft Structures, Tri-State Offset Company, 1965.

TABLE C-I. - POSITIVE 2g MANEUVER LOADS - ONE WING ONLY

94 percent full fuel condition

	Wing air-load		Strut air-load		
A	kN	lbf	kN	lbf	
10	92.12	20 710	-	-	Cantilever wing
20	96.53	21 700	-	-	
25	101.24	22 760	-	-	
30	106.40	23 920	-	-	
10	81.66	18 359	8.77	1 971	Strut-braced wing
20	81.00	18 210	10.59	2 380	
25	81.41	18 301	12.01	2 699	
30	82.76	18 606	13.45	3 024	

TABLE C-II. - ESTIMATED DETAILED WING WEIGHT SAVING, A = 25

Configuration	Estimated wing skin weights					
	Cantilever ①		Strut-braced ②		② - ①	
η	kN	lbf	kN	lbf	kN	lbf
0 → .1	3.08	692	.34	77	-2.74	- 615
.1 → .2	2.67	601	.57	129	-2.10	- 472
.2 → .3	2.38	535	.83	187	-1.55	- 348
.3 → .4	1.92	432	1.16	260	- .77	- 172
.4 → .5	1.50	337	1.11	250	- .39	- 87
.5 → .6	1.09	245	.76	171	- .33	- 74
.6 → .7	.75	168	.55	124	- .20	- 44
.7 → .8	.44	100	.34	76	- .11	- 24
.8 → .9	.24	53	.20	44	- .04	- 9
.9 → 1.0	.12	27	.10	22	- .02	- 5
Σ	14.19	3 190	5.96	1 340	-8.23	-1 850
				Strut weight, table C-III	1.07	240
				(Net saving)	-7.16	-1 610

TABLE C-III. - ESTIMATED STRUT WEIGHTS

	Strut Weight	
A	kN	lbf
10	.62	140
20	.88	198
25	1.07	240
30	1.33	298

TABLE C-IV. - WING STRUT DIMENSIONAL AND WEIGHT DATA

A	No. of strut braces	Strut t/c, percent	Strut length, m (in.)	No. of box I beams	Strut weight, N lbf
20	1	9	6.248 (246)	2	553.8 (124.5)
20	2	9	6.248 (246)	2	397.7 (89.4)
20	1	12	6.248 (246)	2	452.4 (101.7)
20	2	12	6.248 (246)	2	347.0 (78.0)
25	1	9	7.036 (277)	2	734.8 (165.2)
25	2	9	7.036 (277)	2	489.3 (110.0)
30	1	9	7.722 (304)	3	1076.9 (242.1)
30	2	9	7.722 (304)	2	597.8 (134.4)
30	1	12	7.722 (304)	2	717.9 (161.4)
30	2	12	7.722 (304)	2	548.0 (123.2)

NOTE: Strut chord constant .61 m (24 in.) for all aspect ratios.

TABLE C-V. - WING STRUT SIDE-STABILIZING BRACE DIMENSIONAL AND WEIGHT DATA

(a) A = 20, strut chord = .610 m (24 in.), two braces/strut; brace length = 1.016 m (40 in.)

t/c, percent	9				12			
Chord, cm (in.)	5.08 (2)	7.62 (3)	10.16 (4)	12.70 (5)	5.08 (2)	7.62 (3)	10.16 (4)	12.70 (5)
$\bar{t}$, cm (in.)	+	+	.229 (.090)	.117 (.046)	+	.302 (.119)	.127 (.050)	.066 (.026)
Section area, cm^2 ($in.^2$)	+	+	4.671 (.724)	2.987 (.463)	+	4.671 (.724)	2.626 (.407)	1.677 (.260)
Weight/brace, N (lbf)	+	+	12.90 (2.90)	8.23 (1.85)	+	12.90 (2.90)	7.25 (1.63)	4.63 (1.04)
*Weight/brace, N (lbf)	+	+	N/A	N/A	+	N/A	N/A	7.21 (1.62)

(b) Brace length = .508 m (20 in.)

t/c, percent	9				12			
Chord, cm (in.)	5.08 (2)	7.62 (3)	10.16 (4)	12.70 (5)	5.08 (2)	7.62 (3)	10.16 (4)	12.70 (5)
$\bar{t}$, cm (in.)	+	.203 (.080)	.058 (.023)	.030 (.012)	+	.076 (.030)	.033 (.013)	.015 (.006)
Section area, cm^2 ($in.^2$)	+	2.077 (.322)	1.168 (.181)	.748 (.116)	+	1.168 (.181)	.658 (.102)	.419 (.065)
Weight/brace, N (lbf)	+	2.85 (.64)	1.60 (.36)	1.02 (.23)	+	1.60 (.36)	.89 (.20)	.58 (.13)
*Weight/brace, N (lbf)	+	N/A	2.85 (.64)	3.56 (.80)	+	2.18 (.49)	2.89 (.65)	3.60 (.81)

(c) One brace/strut; brace length = .762 m (30 in.)

t/c, percent	9				12			
Chord, cm (in.)	5.08 (2)	7.62 (3)	10.16 (4)	12.70 (5)	5.08 (2)	7.62 (3)	10.16 (4)	12.70 (5)
$\bar{t}$, cm (in.)	+	+	.208 (.082)	.107 (.042)	+	.274 (.108)	.117 (.046)	.058 (.023)
Section area, cm^2 ($in.^2$)	+	+	4.232 (.656)	2.710 (.420)	+	4.232 (.656)	2.381 (.369)	1.523 (.236)
Weight/brace, N (lbf)	+	+	8.76 (1.97)	5.61 (1.26)	+	8.76 (1.97)	4.94 (1.11)	3.16 (.71)
*Weight/brace, N (lbf)	+	+	N/A	N/A	+	N/A	N/A	5.43 (1.22)

* Weights based on .102 cm (.040 in.) minimum skin gauge ; + solid brace, unstable in column compression

TABLE C-V. - Continued

(d) A = 25, two braces/strut; brace length = .991 m (39 in.)

t/c, percent	9				12			
Chord, cm (in.)	5.08 (2)	7.62 (3)	10.16 (4)	12.70 (5)	5.08 (2)	7.62 (3)	10.16 (4)	12.70 (5)
$\bar{t}$, cm (in.)	+	+	.239 (.094)	.122 (.048)	+	+	.135 (.053)	.069 (.027)
Section area, cm^2 ($in.^2$)	+	+	4.890 (.758)	3.129 (.485)	+	+	2.748 (.426)	1.761 (.273)
Weight/brace, N (lbf)	+	+	13.17 (2.96)	8.41 (1.89)	+	+	7.38 (1.66)	4.72 (1.06)
*Weight/brace, N (lbf)	+	+	N/A	N/A	+	+	N/A	7.03 (1.58)

(e) Brace length = .495 m (19.5 in.)

t/c, percent	9				12			
Chord, cm (in.)	5.08 (2)	7.62 (3)	10.16 (4)	12.70 (5)	5.08 (2)	7.62 (3)	10.16 (4)	12.70 (5)
$\bar{t}$, cm (in.)	+	.142 (.056)	.061 (.024)	.030 (.012)	+	.079 (.031)	.033 (.013)	.018 (.007)
Section area, cm^2 ($in.^2$)	+	2.174 (.337)	1.219 (.189)	.781 (.121)	+	1.219 (.189)	.690 (.107)	.429 (.068)
Weight/brace, N (lbf)	+	2.94 (.66)	1.65 (.37)	1.07 (.24)	+	1.78 (.40)	.93 (.21)	.58 (.13)
*Weight/brace, N (lbf)	+	N/A	2.80 (.63)	3.47 (.78)	+	2.09 (.47)	2.80 (.63)	3.51 (.79)

(f) One brace/strut; brace length = .762 m (30 in.)

t/c, percent	9				12			
Chord, cm (in.)	5.08 (2)	7.62 (3)	10.16 (4)	12.70 (5)	5.08 (2)	7.62 (3)	10.16 (4)	12.70 (5)
$\bar{t}$, cm (in.)	+	+	.229 (.090)	.117 (.046)	+	.302 (.119)	.127 (.050)	.066 (.026)
Section area, cm^2 ($in.^2$)	+	+	4.658 (.722)	2.981 (.462)	+	4.768 (.739)	2.619 (.406)	1.677 (.260)
Weight/brace, N (lbf)	+	+	9.65 (2.17)	6.18 (1.39)	+	9.88 (2.22)	5.43 (1.22)	3.47 (.78)
*Weight/brace, N (lbf)	+	+	N/A	N/A	+	N/A	N/A	5.43 (1.22)

* Weights based on .102 cm (.040 in.) minimum skin gauge ; + solid brace, unstable in column compression

TABLE C-V. - Concluded

(g) A = 30, two braces/strut; brace length = 1.016 m (40 in.)

t/c, percent	9				12			
Chord, cm (in.)	5.08 (2)	7.62 (3)	10.16 (4)	12.70 (5)	5.08 (2)	7.62 (3)	10.16 (4)	12.70 (5)
$\bar{t}$, cm (in.)	+	+	.274 (.108)	.142 (.056)	+	+	.152 (.060)	.079 (.031)
Section area, cm^2 ($in.^2$)	+	+	5.619 (.871)	3.600 (.558)	+	+	3.161 (.490)	2.026 (.314)
Weight/brace, N (lbf)	+	+	17.08 (3.84)	9.92 (2.23)	+	+	8.72 (1.96)	5.61 (1.26)
*Weight/brace, N (lbf)	+	+	N/A	N/A	+	+	N/A	7.21 (1.62)

(h) Brace length = .508 m (20 in.)

t/c, percent	9				12			
Chord, cm (in.)	5.08 (2)	7.62 (3)	10.16 (4)	12.70 (5)	5.08 (2)	7.62 (3)	10.16 (4)	12.70 (5)
$\bar{t}$, cm (in.)	+	.163 (.064)	.069 (.027)	.036 (.014)	+	.091 (.036)	.038 (.015)	.020 (.008)
Section area, cm^2 ($in.^2$)	+	2.497 (.387)	1.406 (.218)	.897 (.139)	+	1.400 (.217)	.787 (.122)	.503 (.078)
Weight/brace, N (lbf)	+	3.43 (.77)	1.96 (.44)	1.25 (.28)	+	1.91 (.43)	1.07 (.24)	.71 (.16)
*Weight/brace, N (lbf)	+	N/A	2.85 (.64)	3.56 (.80)	+	2.18 (.49)	2.89 (.65)	3.60 (.81)

(i) One brace/strut; brace length = .762 (30 in.)

t/c, percent	9				12			
Chord, cm (in.)	5.08 (2)	7.62 (3)	10.16 (4)	12.70 (5)	5.08 (2)	7.62 (3)	10.16 (4)	12.70 (5)
$\bar{t}$, cm (in.)	+	+	.249 (.098)	.127 (.050)	+	.330 (.130)	.140 (.055)	.071 (.028)
Section area, cm^2 ($in.^2$)	+	+	5.090 (.789)	3.258 (.505)	+	5.090 (.789)	2.865 (.444)	1.832 (.284)
Weight/brace, N (lbf)	+	+	10.54 (2.37)	6.76 (1.52)	+	10.54 (2.37)	5.92 (1.33)	3.78 (.85)
*Weight, brace, N (lbf)	+	+	N/A	N/A	+	N/A	N/A	5.43 (1.22)

* Weights based on .102 cm (.040 in.) minimum skin gauge ; + solid brace, unstable in column compression

Note: All material is aluminum

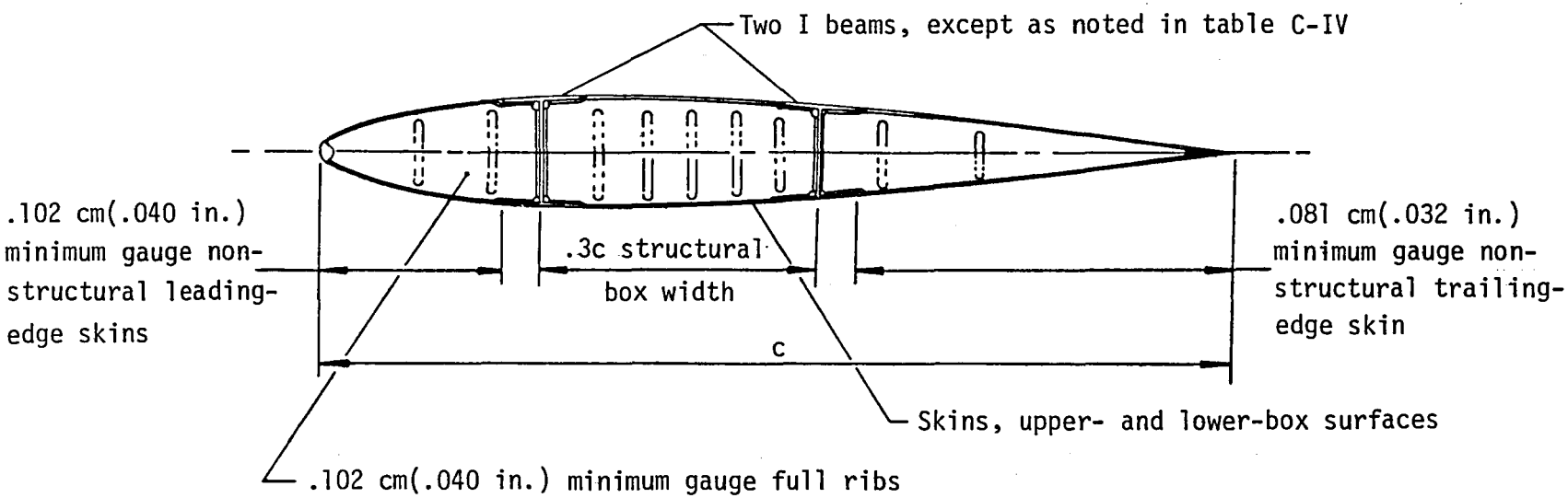

Figure C-1. - Typical wing strut illustrating a two-beam structural box and secondary structure.

1. Report No.	2. Government Accession No.	3. Recipient's Catalog No.
NASA CR-159262		

4. Title and Subtitle	5. Report Date
A STUDY OF HIGH-ALTITUDE MANNED RESEARCH AIRCRAFT EMPLOYING STRUT-BRACED WINGS OF HIGH-ASPECT-RATIO	February 1981
	6. Performing Organization Code
7. Author(s) Paul M. Smith, John DeYoung, William A. Lovell, Jack E. Price, and G. Fred Washburn	8. Performing Organization Report No.
	10. Work Unit No.
9. Performing Organization Name and Address Kentron International, Inc. Hampton Technical Center 3221 N. Armistead Avenue Hampton, VA 23666	11. Contract or Grant No. NAS1-16000
	13. Type of Report and Period Covered Contractor Report
12. Sponsoring Agency Name and Address National Aeronautics and Space Administration Washington, DC 20546	14. Sponsoring Agency Code

15. Supplementary Notes

Technical Monitor: Charles E. K. Morris, Jr.

16. Abstract

A study was conducted to determine whether subsonic aircraft utilizing wings of high-aspect-ratio had range performance and high-altitude capability improvements when compared to a baseline concept. The effect of increased wing aspect ratio on structural weight, system weight, range and altitude performance was determined for configurations with and without strut bracing.

The significant results of the study indicated that an optimum cantilever configuration, with a wing aspect ratio of approximately 26, has a 19 percent improvement in cruise range when compared to a baseline concept with a wing aspect ratio of approximately 10. An optimum strut-braced configuration, with a wing aspect ratio of approximately 28, has a 31 percent improvement in cruise range when compared to the same baseline concept. This large improvement in range capability is mainly due to the estimated reduction in wing weight resulting from use of lifting struts. All configurations assume the same mission payload and fuel. The drag characteristics of the wings are enhanced with the use of laminar flow (NACA 6-series) airfoils. A method for determining the extent of attainable natural laminar flow is presented in an appendix. Methods for preliminary structural design and for aerodynamic analysis of wings with lifting struts are also given in appendices.

17. Key Words (Suggested by Author(s))	18. Distribution Statement
Aircraft design Strut-braced high-aspect-ratio wings Lifting struts Range performance High-altitude capability	Unclassified - Unlimited Star Category 05 - Aircraft Design, Testing and Performance

19. Security Classif. (of this report)	20. Security Classif. (of this page)	21. No. of Pages	22. Price*
Unclassified	Unclassified	91	A05

*For sale by the National Technical Information Service, Springfield, Virginia 22151

End of Document